UNITED NATIONS UNIVERSITY
GEOTHERMAL TRAINING PROGRAMME
Orkustofnun, Grensasvegur 9,
IS-108 Reykjavik, Iceland

Reports 2013
Number 15

BOREHOLE GEOLOGY AND HYDROTHERMAL MINERALISATION OF WELLS MW-09 AND MW-12, MENENGAI GEOTHERMAL FIELD, KENYA

Tito Plimo Lopeyok
Geothermal Development Company
P. O. Box 17700-20100
Nakuru
KENYA
tlopeyok@gdc.co.ke, titolopeyok@yahoo.com

ABSTRACT

Wells MW-09 and MW-12 are exploration/production wells located in the caldera of the Menengai volcano in the Menengai geothermal field. They are both vertical wells. Well MW-09 was drilled to a depth of 2077 m while Well MW-12 was drilled to a depth of 2042 m. This report presents data obtained from analysis of drill cuttings from both wells. Analytical techniques applied, include binocular analysis, petrographic analysis, XRD analysis, and fluid inclusion analysis. The rock units encountered in both wells consist predominantly of trachyte, tuffs, pyroclastics, and a syenitic intrusion at depth. The top section of the well consists of blocky post-caldera trachyte lavas overlain by a thin layer of pyroclastic deposits. A thick layer of tuff encountered at 200-300 m marks the boundary between pre- and post-caldera lavas. Hydrothermal minerals in Menengai occur as replacements of primary minerals or as vein and vesicle fillings. The main hydrothermal minerals observed in both wells include: zeolite, chalcedony, calcite, pyrite, quartz, wollastonite, and actinolite. Based on alteration mineral assemblages and clay analysis, three alteration mineral zones were identified. They are: smectite zeolite zone, quartz-illite zone, and actinolite-wollastonite-illite zone. The appearance of actinolite at 1364 m in Well MW-09 and at 1922 m in Well MW-12, indicates formation temperatures over 280°C.

1. INTRODUCTION

Menengai is a high-temperature geothermal field situated north of Lake Nakuru on the floor of the central Kenyan Rift (Figure 1). It is comprised of three volcanic centres: Menengai caldera, the Ol'rongai volcano to the northwest, and the Olbanita plains and parts of the Solai tectonovolcanic axis (TVA) to the northeast (GDC, 2010). Deep geothermal wells have been drilled in the Menengai caldera and proved the existence of a geothermal resource. At the time of writing this report, 15 wells have been drilled. Wells MW-09 and MW-12 are the ninth and twelfth exploration wells to be drilled in the Menengai geothermal field, respectively, both sited within the caldera. They are vertical wells drilled to depths of 2077 and 2042 m, respectively. Well MW-09 is located at coordinates E172848, N9977301 at an elevation of 2105 m a.s.l. Well MW-12 is located at coordinates E173573, N9976446 at an elevation 2132 m a.s.l. The wells were aimed at tapping from the NE-SW striking faults and the NNW-SSE structures associated with the Solai and Molo tectonovolcanic axes, respectively.

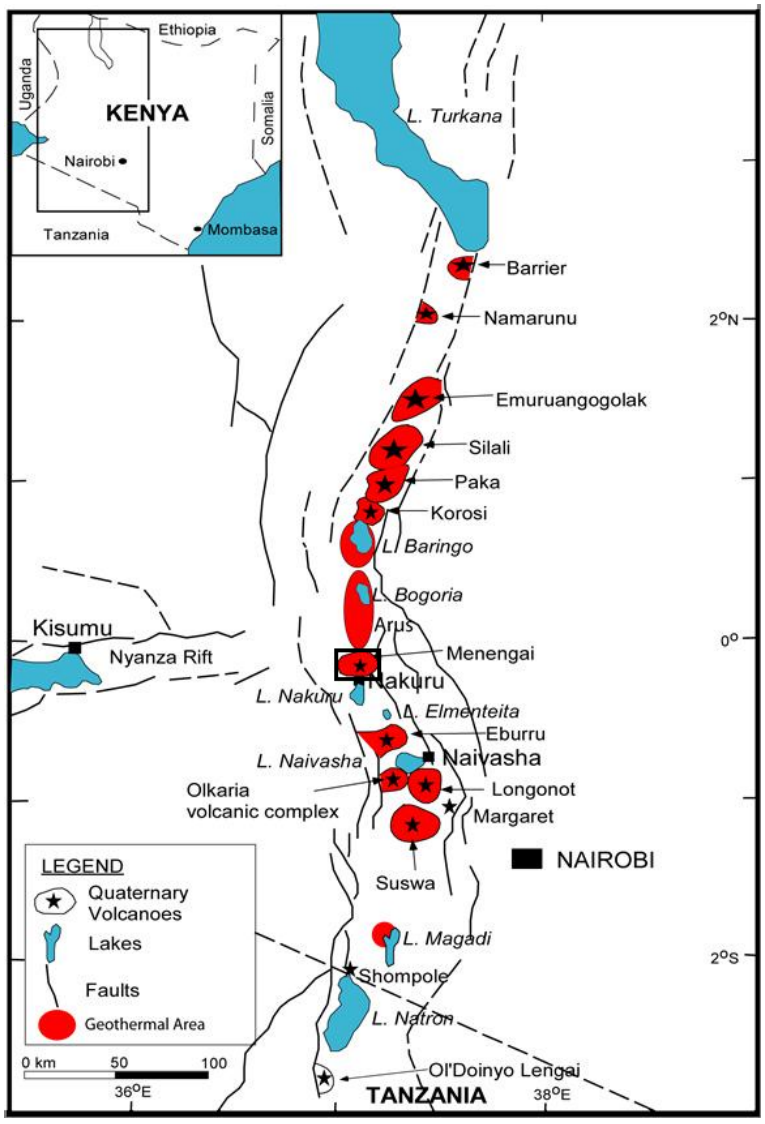

FIGURE 1: Map showing the location of Menengai (obtained and modified from Omondi, 2011)

The objectives for drilling the wells was to further explore and determine subsurface geology, hydrothermal alteration, the nature of the reservoir, chemical characteristics, and the depth to the resource. This report presents data acquired from analysis of rock cuttings from both wells. The project report was carried out as a partial fulfilment of a six month training course at the United Nations University Geothermal Training Programme (UNU-GTP).

2. GEOLOGY

2.1 Regional geology

The East African Rift system is an active continental rift zone in East Africa that is characterized by intense tectonism and volcanism. It is a series of aligned successions of adjacent individual tectonic basins which are several thousand kilometres long. The basins are generally bordered by uplifted shoulders (Chorowicz, 2005). Each basin is controlled by faults and forms a graben or a trough, nearly one hundred kilometres long, and a few tens of kilometres wide, which is either empty or filled with sediments and/or volcanic rocks (Chorowicz, 2005). The graben basins are linked by intracontinental transforms and segmented by transfer zones and accommodation zones. The East African Rift system has two main branches: the western and eastern branches. The western branch runs over a distance of 2200 km from the Afar triple junction to Northern Tanzania while the eastern branch runs over 2100 km from Lake Albert in Uganda to Lake Malawi in Malawi.

Two mantle plumes occur beneath the East African Rift system. The northern plume corresponds to the Ethiopian dome while the southern one corresponds to the Kenyan dome. However, the number of mantle plumes influencing magmatism and tectonics in the East African Rift has generated an extensive debate but with most authors favouring a two plume model (Ebinger and Sleep, 1998; George et al., 1998; Rogers et al., 2000). There is a general consensus, from geophysical, petrological, and geochemical evidence, that the Afar mantle plume underlies the Ethiopian plateau. The uncertainty is mainly in regard to the Kenyan and Tanzanian segments of the Rift system. It is suggested that magmatism was related to the presence of hot mantle plume material beneath the site of the present rift with such a mantle having a potential temperature of up to 1500°C (Mechie et al., 1997). Figure 2 shows a map of Africa illustrating elevated grounds of more than 1200 m above sea level. The elevated areas are mainly associated with a mantle that influences magmatism and tectonics in the East African Rift system.

The Kenya Rift Valley forms a segment of the eastern branch of the East African Rift system. It runs from Lake Turkana in the north to Lake Natron (Tanzania) in the south where the rift splays southwards to form the Northern Tanzanian divergence. Magmatism in the Kenyan Rift is mainly related to the rise of a plume that is focused beneath a weak zone that marks the boundary between the Tanzanian craton and the adjacent Proterozoic mobile belt (Smith, 1994). Along the 40-80 km wide rift graben, several Quaternary volcanic centres are formed. The volcanoes are rooted on open fractures such as tension joints, tail-cracks or tensional releasing bends (Korme et al., 1997). Most of the volcanoes are eruptive with one or more explosive or effusive eruptions that initiated caldera collapse. Volcanic material from these volcanic centres coupled with Quaternary sediments virtually covers the whole rift floor. The evolution of the Kenyan Rift started in early Miocene (30-35 Ma) at the Turkana Rift in northern Kenya (Baker et al., 1971, 1972; Smith, 1994; Lagat et al., 2005). This is where the earliest volcanic rocks in the Kenyan Rift have been found (Macdonald et al., 2001). It marked the onset of magmatism that has since propagated towards the south through the Central Rift and the southern Kenyan Rift before finally reaching northern Tanzania 5-8 Ma ago (Baker and Wohlenberg, 1971; Baker et al., 1972). The high elevation at the central Kenyan Rift may be the result of dynamic or thermal uplift that is caused by an underlying mantle plume (Baker and Wohlenberg, 1971). Seismic studies also indicate crustal thickening resulting from intense magmatic activity that may also contribute significantly to the uplift (KRISP working group, 1987). Crustal thickness beneath the Kenyan Rift is estimated to be 30–35 km (e.g. Mechie et al., 1997).

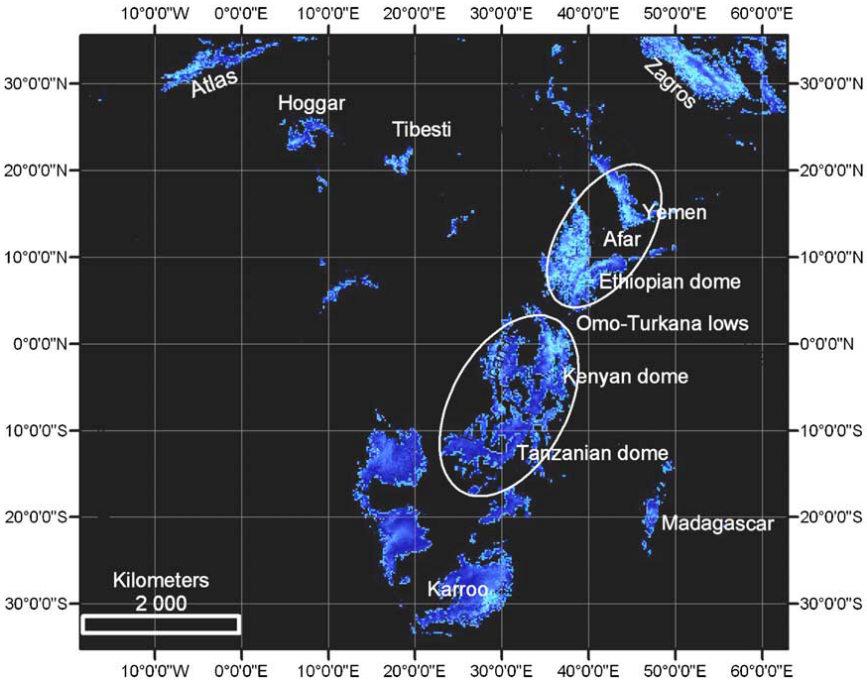

FIGURE 2: Map of Africa showing elevated surfaces higher than 1200 m; the two circles represent the Ethiopian and Kenyan domes (Chorowicz, 2005)

The basement to the Kenyan Rift (Figure 3) is complex and is divided into three zones: the Archaean Tanzanian craton, the late Proterozoic Panafrican Mozambique belt and a zone of craton margin which was reactivated during the Panafrican orogeny (Smith and Mosley, 1993).

The Kenyan Rift is divided into three sectors: northern, central and southern rifts. The central Kenyan rift, at Menengai, is characterized by a sharp turn in rift direction. This marks the boundary between the northern Kenyan Rift Valley and the Central Rift. The Central Kenyan Rift segment is set in the middle of the Kenyan dome. The general elevations of the rift floor rise from 1050 m in the north, to 2100 m in the centre (Central Rift), and steps down progressively southwards to 600 m at Lake Natron. Smith and Mosley (1993) explain the sharp bend of the rift at Menengai to be an intersection of the rift with a large NW-striking basement structure called the Aswa lineament. Simiyu and Keller (1997) associate the sharp bend with the extent of contact between the Archaean Tanzanian craton and the orogenic belt. A N80°E trending Nyanza half-graben branches with the Central Kenyan Rift at Menengai (Figure 3), and disappears westward under Lake Victoria. The Menengai volcano is situated at a triple junction between the northern Kenyan, central Kenyan and Nyanza rifts, almost at the centre of the Kenya dome.

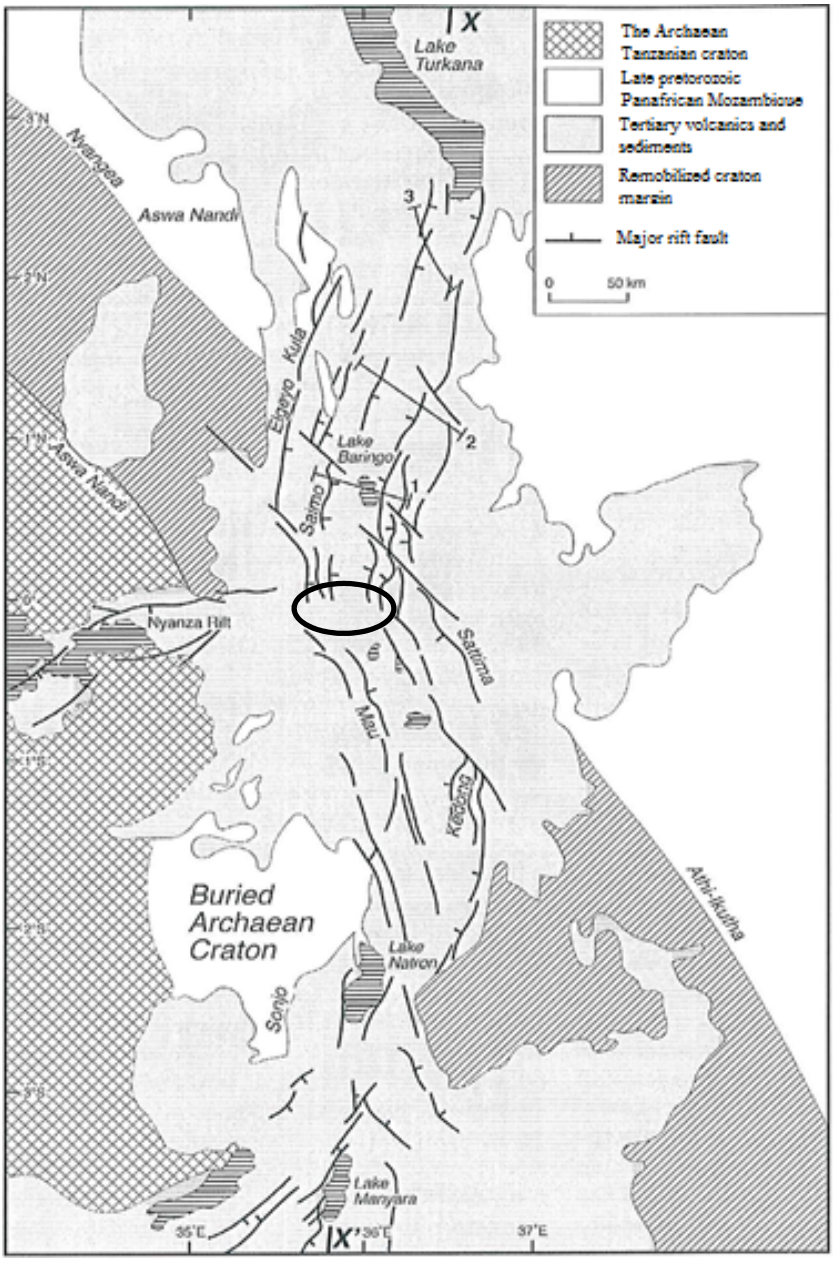

FIGURE 3: Structural framework of the Kenyan Rift; the circle marks the location of Menengai (modified from Smith and Mosley, 1993)

2.2 Geology of Menengai

The Menengai geothermal field region comprises Menengai volcano, the Ol'rongai volcanoes, the Olbanita plains, and parts of the Solai TVA to the northeast (GDC, 2010) covering an area of approximately 950 km² (Figure 4). Menengai is one of the Quaternary volcanoes formed on the axis of the Kenyan Rift (Figure 1). It is a trachytic central volcano that is underlain by a high-level magma chamber. The activity in the volcano started 0.2 Ma ago with the formation of a broad low angle trachytic lava shield (Leat, 1984). The activity continued in the Pleistocene, with the formation of a caldera, to more recent activity that has given rise to the flows on the caldera floor (Macdonald et al., 1970). The surface geology is dominated by recent (post-caldera) lavas especially within the caldera, pyroclastics and ignimbrite sheets on the northern flanks and alluvial sediments on the surrounding rift floor (Figure 4). The geology of Menengai can be divided into three main phases: pre-caldera volcanics, syn-caldera activity, and post-caldera activity. The first phase, the pre-caldera phase, is associated with the formation of the shield and the eruption of lavas that preceded the collapse of the caldera. The pre-caldera lavas were covered by later syn- and post-caldera volcanics and are, therefore, not seen on the surface. The caldera wall, however, exposes a good sequence of the shield building lavas with minor airfall tuff intercalations. The oldest exposed pre-caldera lava yielded a K-Ar date of 0.18±0.01 Ma (Leat, 1984). Based on the fact that the outcrop is exposed at an altitude 50 m higher than the inferred shield base, it is presumed that it must have been erupted during the early shield building stage. This, therefore, suggests that activity at Menengai started shortly before 0.18 Ma. On the north-western flank of the Menengai shield, scoraceous airfall tuffs of pre-caldera age are exposed around the Ol'rongai volcanic centre. The total volume of the pre-caldera volcanics is estimated to be 29 km³, mostly consisting of lava (Leat, 1984).

The second phase, the syn-caldera activity, is associated with the caldera collapse. The incremental caldera collapse is believed to have occurred in two episodes (Leat, 1984; Macdonald and Scaillet,

2006). The formation of the 11.5×7.5 km large caldera was accompanied by the eruption of two ash flow tuffs. Each of the tuff layers is underlain by a pumice deposit and separated by a thin layer of sediments, indicating a short quiescence period between the eruptions. The collapse is mainly associated with the second ash flow eruption. The ash flow tuffs covered an area of approximately 1350 km² with an estimated volume of 50 km³ (Leat, 1984). Ash samples (cores) of the syn-caldera activity have yielded a carbon date between 12,850-29,320 years BP. This, therefore, estimates the probable age of the Menengai caldera.

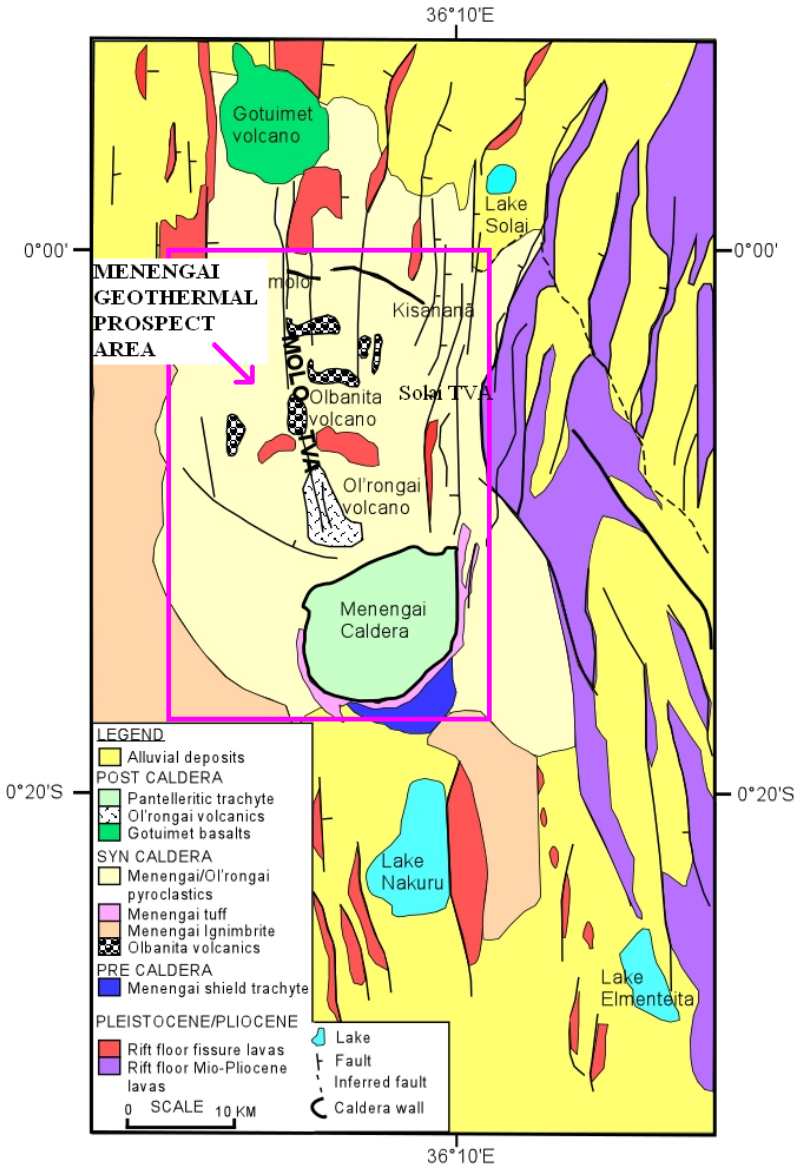

FIGURE 4: Geological map of Menengai (GDC, 2010)

The third phase, the post-caldera activity, mainly involved an eruption of recent lavas and ash deposits from vents within the caldera. An estimated 23 km³ of lava from about seventy lava flows cover almost the entire caldera floor (Leat, 1984). The post-caldera lava pile is estimated to be about 300 m thick. Ash deposits cover areas around Menengai and are more widespread on the western flanks, probably due to westward direction of prevailing winds during the eruptions. The ash deposits are also interbedded with lava flows on the caldera floor. Other post-caldera units include lake sediments found inside the caldera and unconsolidated scoria erupted from trachytic cinder cones found in the southern part of the caldera floor and rim.

2.3 Tectonic structures of Menengai

The tectonic setting of Menengai is complex. Menengai is set at a point where the Kenyan Rift abruptly takes a sharp change in direction. This change is associated with the contact between the Tanzanian craton and orogenic belts (Simiyu and Keller, 1997). The bend is also associated with the Aswa lineament intersecting the Kenyan Rift (Smith and Mosley, 1993). It also marks a triple junction where the Nyanza half-graben (failed rift) branches with the Kenyan Rift (Burke and Dewey, 1973).

According to Chorowicz, (2005), Menengai developed on a possible tail-crack end structure (Figure 5) at the southern end of a complex N-S striking fault zone. This N-S trending fault zone defines the Solai tectonovolcanic axis. Most of the post-caldera lava flows erupted from along the arched tail-crack structure that developed on the western part of the Solai TVA end. The Solai TVA is parallel to, and

continuous with, a swarm of young faults which cut the rift valley floor between Menengai and the equator (Leat, 1984). There is also an indication from the tail-crack structure that the N-S striking zone of normal faults has a dextral strike-slip throw component (Chorowicz, 2005).

FIGURE 5: Tail-crack end of the N-striking fault zone in Menengai (Chorowicz, 2005)

Menengai caldera is an elliptical depression with major and minor axes measuring approximately 11.5 km and 7.5 km, respectively (GDC, 2010). The general NE-SW orientation (Figure 6) and elliptical shape depicts extensional tectonics in Menengai with the main rift trough trending N-S north of Menengai and NNW-SSE south of Menengai. Mibei (2012) relates the extensional tectonics on the caldera to spatial variations in the crustal stress regime, as illustrated by different orientations of faults north of the caldera.

A NW-SE trending ridge on the northwest part of the Menengai shield defines the Ol'rongai tectonic structure that represents part of the larger Molo TVA (Geotermica Italiana, 1987). This structure extends northwards past the Goitumet volcanic centre and possibly southwards into the Menengai caldera. These two tectono-volcanic axes, Molo TVA and Solai TVA, are important in controlling the permeability in the geothermal system.

2.4 Geothermal exploration and geoscientific aspects of Menengai

A detailed study of the geothermal assessment of the Menengai field was carried out by KenGen and the Kenyan Ministry of Energy in 2004. The purpose of the investigations was to determine the existence of a geothermal system in Menengai and recommend locations for exploratory drilling. The study involved geological, geophysical and geochemical surveys. Integrated results of the studies indicated the existence of a hot, ductile, and dense body centred beneath the Menengai caldera. The study estimated that the high-temperature part of the resource covers an area of about 48 km^2 (KenGen, 2004). More detailed work involving all the geoscientific disciplines was carried out by the Geothermal Development Company (GDC) in 2010. Based on the results of the study, exploratory wells were sited. Drilling started in February 2011 and is still ongoing. At the time of writing this report, 15 wells have been drilled.

An iso-resistivity map plotted from 1D joint inversion of magnetotelluric (MT) and transient electromagnetic (TEM) data indicates a conductive body of less than 5Ωm at 2000 m.b.s.l, centred under the southern caldera floor, and a smaller anomaly at the centre of the caldera (Figure 7).

Result from micro-seismic studies indicated that seismic events are concentrated within the Menengai caldera, around the central to the southern part of the caldera, by the northeast caldera wall and the Olbanita area to the northwest of the Menengai caldera where the events are also shallow (Simiyu, 2010). The events occur along two trends. The first follows the rift axis in a NNW-SSE trend cutting through Olbanita, Menengai and towards Lake Nakuru in the southeast. The second trend is parallel to the Nyanza Rift axis in a NE-SW direction along the major axis of the caldera from Bahati on the Aberdare ranges, through the caldera, Nakuru town and Rongai. Figure 8 shows a NW-SE seismic event section with a depth distribution across Olbanita and Menengai caldera. Vp/Vs ratios indicate the caldera area to have lower velocity ratio formations with deeper horizons, suggesting a high temperature, low pore pressure and vapour dominated system (Simiyu, 2010).

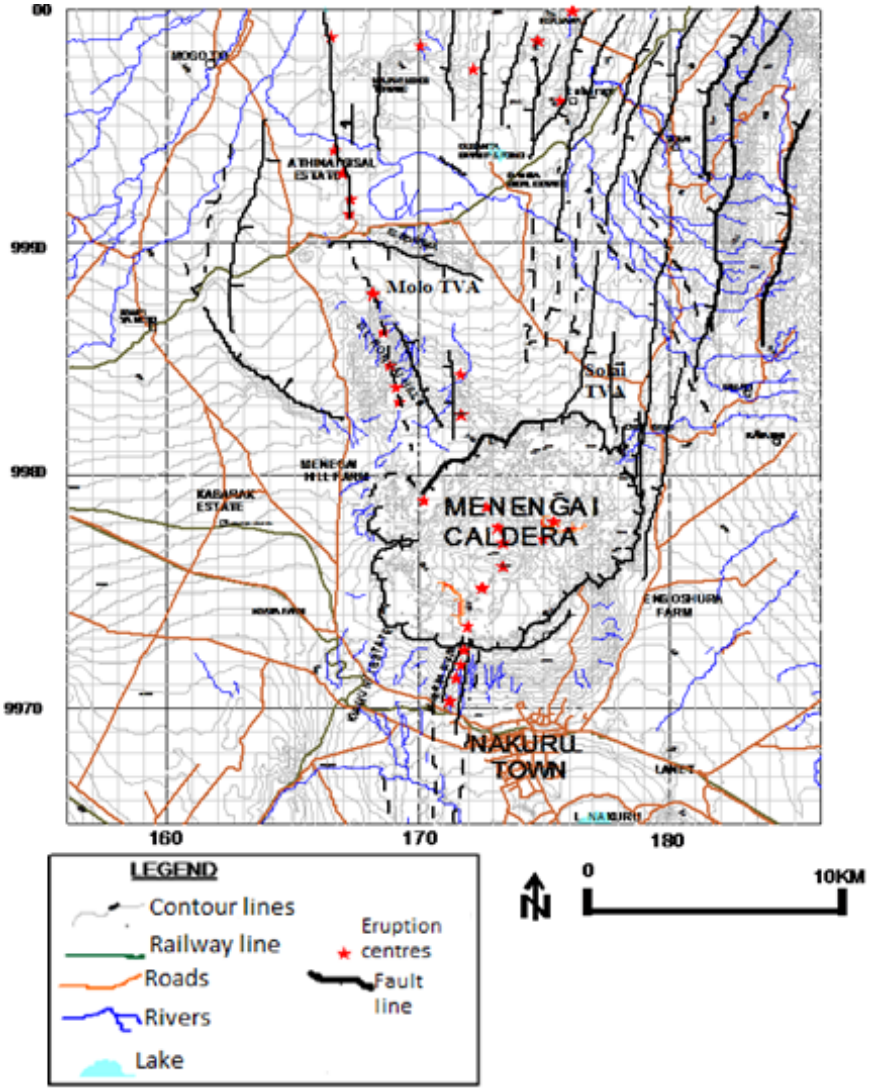

FIGURE 6: Structural map of Menengai (GDC, 2010)

The seismic activity is intense with shallow events centred on the Menengai caldera. This zone of shallow events is, therefore, presumed to indicate the heat source for the geothermal system.

Geochemical studies in Menengai revealed high CO_2 values (>2.5%) along a narrow belt running NW-SE (along Molo TVA) while other areas exhibit values lower than 1 %. High carbon dioxide concentration in the soil gas was observed around Ol'rongai Hill, in the central part of the caldera and in the south-western part of the caldera, indicating good permeability. High absolute values of Rn-220 gases in the soil and fumaroles were measured in the northern and north-western parts of Menengai and in the caldera, indicating enhanced permeability. The ratio of the Rn-220/CO_2 gases indicated high values in the northern parts of the field and within the caldera. These areas also showed high CO_2 and Rn-220 absolute values. The soil temperature measurements taken at a depth of 0.7 m showed a higher-temperature anomaly in the caldera, especially around the fumaroles. CO_2, H_2 and H_2S gas geothermometry for the Menengai fumaroles gave calculated temperatures of above 250°C. From the temperature estimation using the gas geothermometers, it is presumed that the reservoir temperatures beneath Menengai caldera are over 250°C (GDC, 2010).

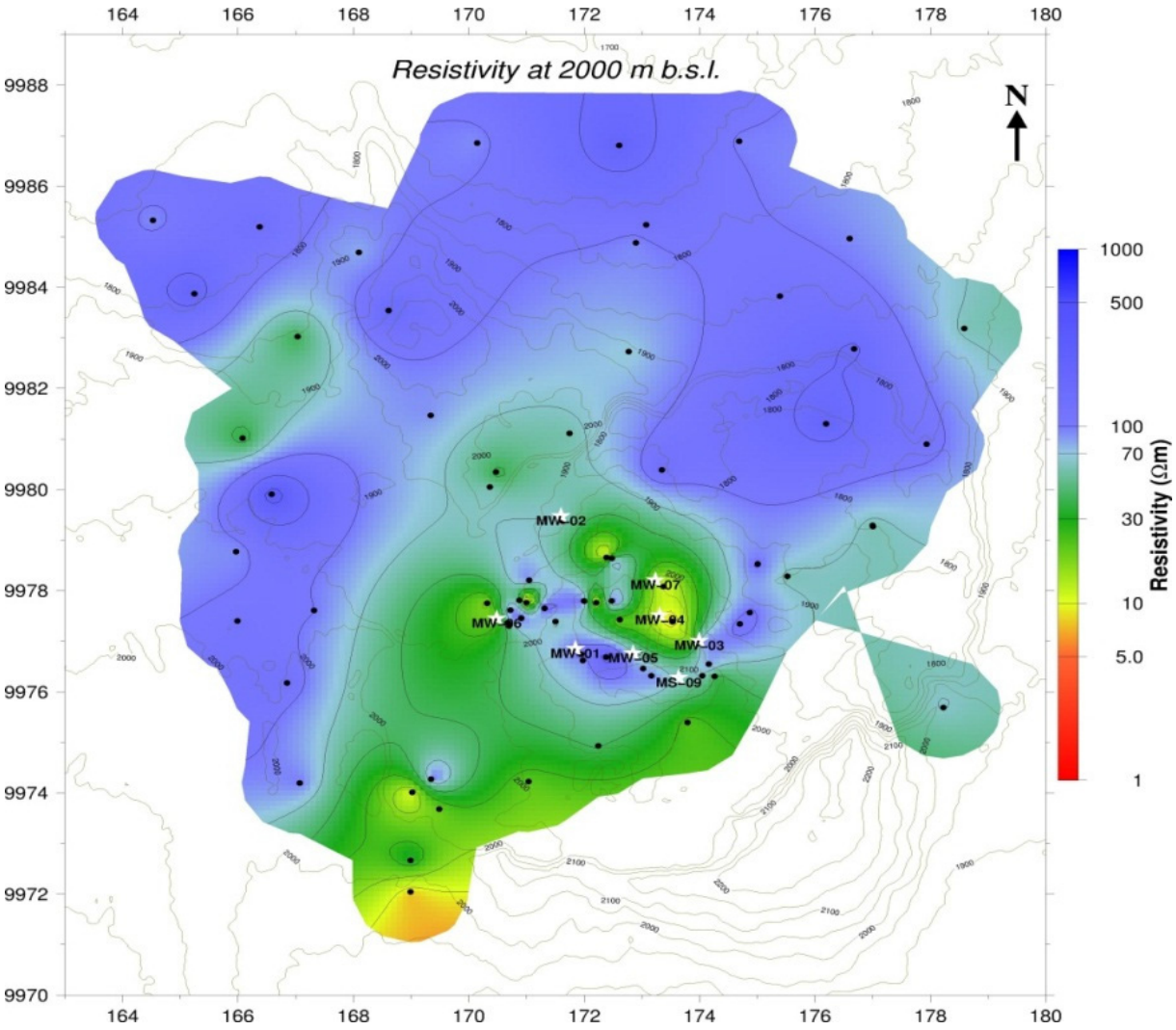

FIGURE 7: Iso-resistivity map at 2000 m.b.s.l. of the Menengai field; black dots denote 1D inversion models while the white stars represent Menengai wells (Gichira, 2012)

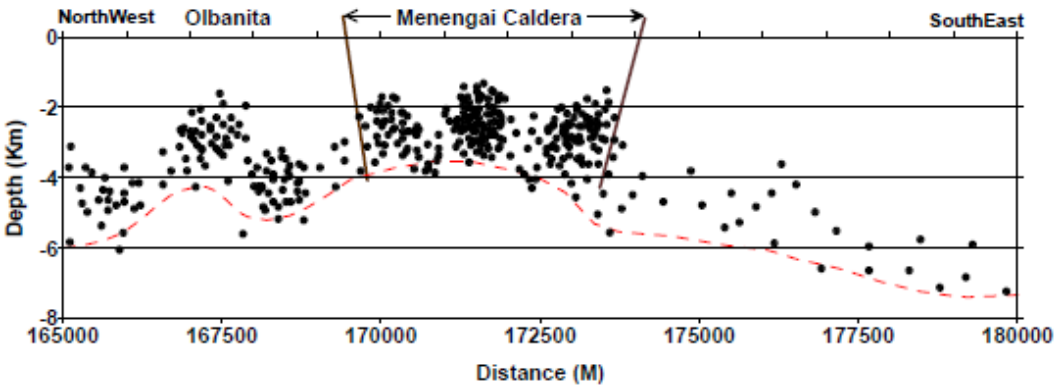

FIGURE 8: The distribution of seismic events in Menengai (Simiyu, 2010)

3. SAMPLING METHODOLOGY AND ANALYSIS

Cuttings from Menengai wells were sampled at two metre intervals during drilling after which a preliminary binocular analysis was performed at the rig site by the rig geologists. The main features identified include: the lithology penetrated, the rock texture, fractures, alteration minerals and the intensity of alteration. The results from the preliminary analyses supported the determination of casing depths as well as in advising the drilling crew and engineers on various geotechnical aspects. The samples were then taken to the GDC laboratory, washed, dried, packed and stored systematically for easy retrieval. Samples of interest from selected depths were identified and thin sections prepared for further petrographic analysis. For the purpose of this project, portions of cutting samples from all the available depths for Wells MW-09 and MW-12 were sent to the Iceland GeoSurvey (ISOR) laboratories in Iceland for detailed analyses. The four main analytical techniques employed were: binocular analysis, petrographic spectroscopy, X-ray diffraction analysis, and fluid inclusion analysis.

3.1 Binocular analysis

All the samples were prepared for binocular analysis. The samples were carefully washed with clean water to remove impurities and dust to enhance visibility. The aim of this analysis was to identify the lithology, texture, alteration mineralogy, degree of alteration, and fracturing. The samples were analysed using an Olympus SZX12 binocular microscope and the properties noted include: the colour of the rock, grain size, texture, vein filling if present, alteration mineralogy, and degree of alteration; from these observations, the rock types and their properties were identified. Samples of interest were selected for XRD analysis. Platy calcite and quartz grains from different depth ranges in both wells were picked for fluid inclusion geothermometry.

3.2 Petrographic microscopy

Based on preliminary binocular analysis performed at the rig site, representative samples from different depths and lithologic units in both wells were selected for petrographic analysis. A total of 66 thin sections, 21 from Well MW-09 and 45 from Well MW-12, were prepared at the GDC laboratories. The thin sections were analysed using a Leitz Wetzler petrographic microscope. The purpose was to confirm rock types, grain sizes, rock textures, and to identify additional alteration minerals that were not observed during the examination with the binocular microscope. The order at which the alteration minerals were formed was also noted when possible.

3.3 X-ray diffraction analysis

A total of 36 samples, 27 from Well MW-09 and 9 from Well MW-12, were selected for XRD clay analysis in order to identify the alteration zones. Untreated, glycolated and heated samples were evaluated to classify the clay types found in the wells. The clay analyses were carried out using a Bruker D8 focus XRD machine. Results of the XRD analysis for both wells are summarized in tables in Appendices I and II, and examples given in Appendix III.

Portions of cuttings from selected samples were scooped and mixed with water in test tubes. The mixtures were shaken for 4-5 hours to dissolve and extract clay from the cuttings. A few drops of water from each of the dissolved drill cutting samples were placed on separate glass slides which had been washed previously with an organic solvent, acetone and dipped in a glycol solution for 24 hours. The samples in the test tubes were left to settle for 12 hours. The clay samples were first run in the X-ray diffractometer and the peaks recorded. The glycolated samples were subsequently run in the X-ray diffractometer and the peaks were recorded. The clay samples were heated to 550°C before performing the third run in the X-ray diffractometer and the peaks were recorded. For each sample, three peaks, each from the corresponding runs, were recorded. The main aim for the analysis was to identify clays,

zeolites and actinolite alteration minerals, establish the alteration zonation and to further deduce the alteration temperatures.

3.4 Fluid inclusion analysis

Based on the measured temperature logs and binocular analysis, quartz and platy calcite mineral grains were selected from two depth ranges in each well. A fluid inclusion analysis for the mineral grains was undertaken to predict the temperatures at which the minerals were formed (primary mineral) or when the fractures healed (secondary mineral). The mineral grains were heated using a Linkam THSMG 94 stage and the temperatures at which bubbles disappeared were noted. The temperature measurements were recorded at 5°C intervals. The temperatures at which the bubbles disappeared corresponded closely to the temperature conditions at which the fluids were trapped in the crystal. This is referred to as the homogenisation temperature (T_h). Fluid inclusion geothermometry, when compared with results from alteration mineralogy and well temperature measurements, provides important information on the thermal history of a geothermal system. It provides evidence as to whether a geothermal system is heating, cooling or is in equilibrium.

4. BOREHOLE GEOLOGY

4.1 Drilling wells

Wells MW-09 and MW-12 are the ninth and twelfth wells, respectively, to be drilled in the Menengai geothermal field. They are both vertical wells located inside the caldera (Figure 9). The wells were

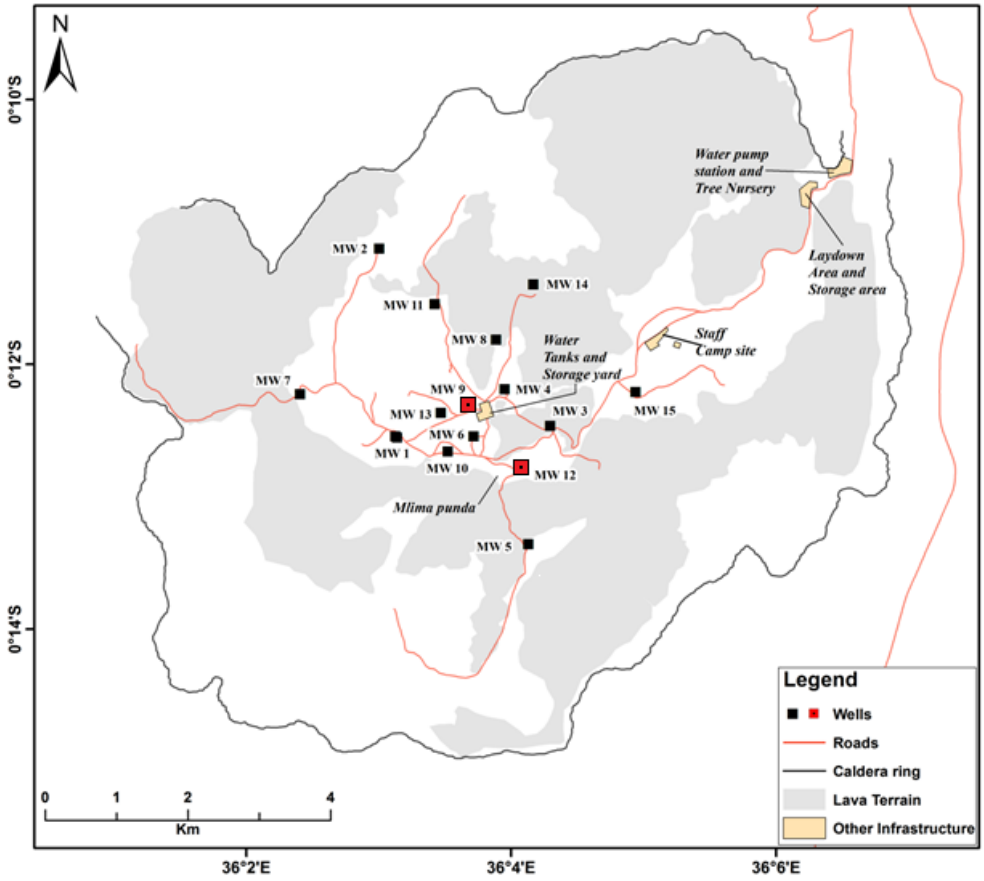

FIGURE 9: Locations of wells MW-09 and MW-12

aimed at tapping from the NE-SW striking faults and the NNW-SSE structures associated with Solai and Molo tectonovolcanic axes (Figure 6).

4.1.1 Well MW-09

The well was spudded on 17th July, 2012 and completed on 29th October, 2012. It took 105 days to complete drilling the well, reaching a depth of 2077 m from the cellar top (CT) (Figure 10). The target depth according, to the well prognosis, was set at 2200 m. However, the drilling was terminated at 2077 m after persistent circulation losses from 2036 to 2077 m, and a significant increase in torque. An effort was made to regain circulation by employing underbalanced drilling, but this proved to be futile. Based on experience from previously drilled wells within the field, it was found necessary to terminate the well at this point. The drilling of Well MW-09 was executed in four phases from the start to the successful completion (Table 1).

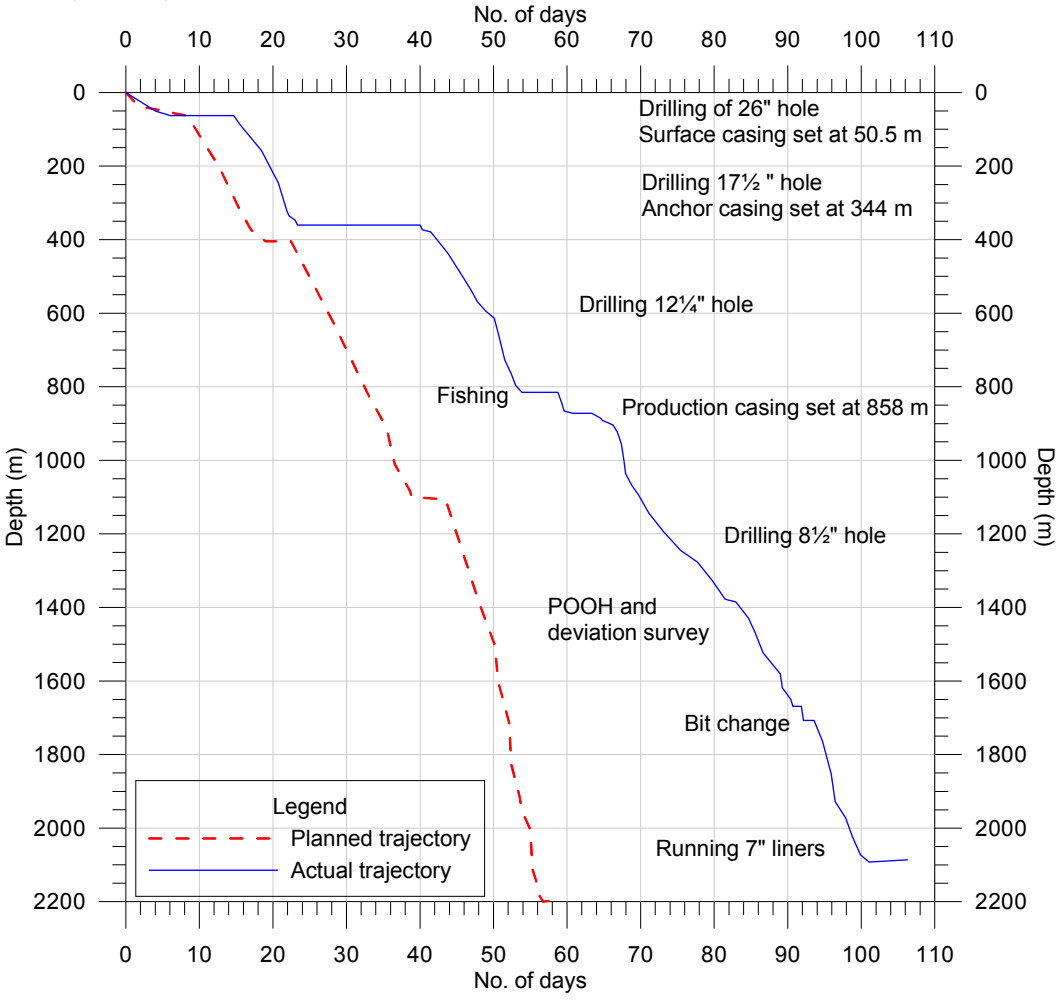

FIGURE 10: Drilling progress of Well MW-09

For the first phase, a 26" surface hole was drilled to a depth of 50 m CT. The drilling fluid used was mud for the first 10 m and thereafter changed to water with high viscosity mud sweeps at regular intervals. The 20" surface casing was set at 50 m. Total loss of

TABLE 1: Drilling phases and depths of Well MW-09

Drilling phase	Drill bit diameter	Casing diameter	Drilled depth (m)
First	26"	20"	50
Second	17 ½"	13⅜"	344
Third	12 ¼"	9⅝ "	858
Fourth	8 ½"	7" Slotted liners	2077

returns was experienced from 2-14 m and 16-26 m.

Circulation of returns was fairly good in the bottom half of the section. Primary and secondary cement jobs were done. Cement return was received on the surface after performing sixteen backfill cement jobs. A total of 180.34 tons of cement was consumed in this section.

For the second phase, a 17½"hole was drilled to a depth of 344 m CT where the 13⅜"casing was set. The upper part of this section was drilled with mud and thereafter with water and occasional mud sweeps to the bottom of the section. This intermediate section was characterized by partial losses from 50-131 m, total loss of circulation from 131-338 m and good circulation of returns from 338-344 m. Primary cementing was done and cement was received on the surface after performing nine backfill cement jobs, consuming a total of 110.75 tons of cement.

The 12¼" hole, the third phase, was drilled to a depth of 858 m CT and the 9⅝" production casing was set at 856 m. The drilling fluid used was mud from 344-800 m and water with gel sweeps at regular intervals from 800-858 m. A 9⅝" casing was run in to a depth of 858 m and a cement job was performed. Cement was received on the surface after the first backfill cement job, consuming 54 tons of cement. Circulation of returns was fairly good in this section except for a total loss experienced at 542-552 m and occasional intermittent losses. The fourth and final phase of drilling was the $8^{1}/_{2}$" production section which was drilled to the total depth of 2077 m, after which the 7" slotted liner was run in. Circulation of returns in this section was relatively good except for intermittent losses and partial loss of circulation at 882-886, 890-892, 894-900, 902-904, 908, 950-954, 964-968, 1022, 1058, 1072, 1042, 1158, 1368, 1382, 1482, 1694-1700, 1722, 1862-1866, 1978, 1996, 2008, 2044, 2054, and a total loss from 2060 m to the bottom of the well. The liner was set hanging at 801 m, 55 m above the production casing shoe.

4.1.2 Well MW-12

The well was spudded on 14th October 2012 and completed on 16th January 2013. It took 93 days to complete drilling the well (Figure 11). The target depth was set at 2200 m but as the drill string got stuck, drilling was terminated at 2042 m. A summary of casing depths, bits and casing diameters for the four phases of well drilling is shown in Table 2. The surface hole was drilled with mud to a depth of 48 m with good returns of circulation until 38 m depth where total loss of circulation was encountered and was persistent until the casing depth of 48 m had been reached. The 20" surface casing was run in and a cement job was performed. Cement returns were received on the surface after primary cementing and six backfill cement jobs. A total of 96.28 tons of cement was used in this section.

TABLE 2: Drilling phases and depths of Well MW-12

Drilling phase	Drill bit diameter	Casing diameter	Drilled depth (m)
First	26"	20"	48
Second	17 ½"	13⅜"	358
Third	12 ¼"	9⅝ "	850
Fourth	8 ½"	7" Slotted liners	2042

The second phase was drilled with a 17½" bit to a depth of 358 m, where the anchor casing was set. Mud was used as drilling fluid from 48 to 332 m and then water to the bottom of the section. Circulation returns were rather poor with frequent circulation losses that prompted ten cement plug jobs and/or use of lost circulation material (LCM) to heal the losses and regain circulation. A total volume of 164.68 tons of cement was consumed in this section, 76.89 tons for the casing and 87.79 tons for the plug jobs.

The third phase, a 12¼" hole, was drilled to a depth of 850 m and the production casing was set at 843 m. The section was initially drilled with mud to a depth of 444m, before switching to aerated drilling to the bottom of the section. Circulation of returns was generally not good in this section. Major circulation losses were encountered at 436-478, 526-552, 562-588, 594-616, 680-690, and 736-806 m while a total loss was encountered at 436-478 m. Cement plug jobs were performed where total loss was experienced

in an attempt to heal the loss. Primary cementing and two backfills were completed before returns were received on the surface. A volume of 96.86 tons of cement was consumed in this section. A volume of 79.69 tons of cement was used to cement the 9⅝" casing while 17.17 tons was used to perform plug jobs.

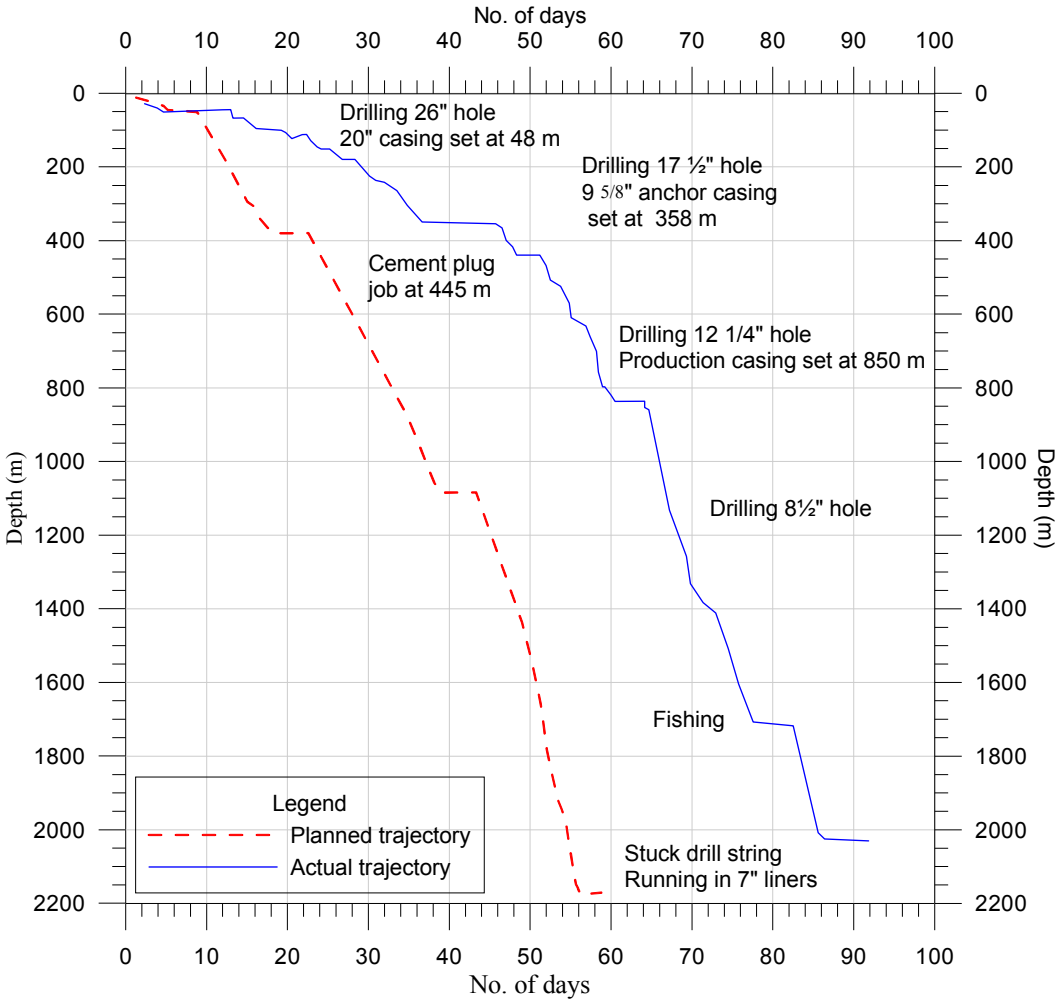

FIGURE 11: Drilling progress of Well MW-12

The final phase was drilled using an 8½" bit to a depth of 2042 m with aerated water and foam. Circulation returns were good throughout the column. No major geotechnical problems were encountered in this section. The drill string got stuck at 2042 m for four days before it was freed. After the string was unstuck, a 7" slotted liner was run in to the bottom of the hole. The liner was set hanging at 813 m, 30 m above the production shoe casing.

4.2 Stratigraphy

The stratigraphy of Menengai Wells MW-09 and MW-12 is dominated by trachyte with occasional tuff intercalations. Pyroclastics and a syenitic intrusion at the bottom section of the wells are the only other formations encountered.

Pyroclastics: These occurred at two levels in Well MW-09, on the surface (0-2 m) and from 342-346 m, and once in Well MW-12, from 8-12 m. They are brownish grey in colour, oxidized and unaltered. The rock contains a mixture of brownish tuff, pumice, trachyte, and obsidian (only in the top section). The tuff is vesicular with some of the vesicles filled with amorphous silica lining and zeolites.

Trachyte: In both wells trachytes occurred from the surface to the bottom of the well with intermittent tuff intercalations. Trachytes vary widely in terms of colour, texture and mineralogical composition. It varies from light grey, greenish grey, brownish grey to dark grey in colour, fine to medium grained in grain size. The texture varies from equigranular, to weakly porphyritic to strongly porphyritic. The porphyritic nature and their dissimilarity occur as a result of varying phenocryst sizes and quantity. The main phenocrysts are pyroxenes and sanidine feldspars. The groundmass is mainly made up of feldspars that show trachytic flow textures and, in some instances, spherulitic textures. The lower section of the wells is mainly composed of medium to fine grained trachytes.

In the upper sections of the wells, the trachyte is fresh, grey to dark grey in colour, fine grained and porphyritic. It is blocky in nature and highly fractured and, therefore, circulation fluid was lost in this section. The enormous amount of primary cement pumped during the surface casing and the number of backfills in the section gives a picture of how fractured the formation is. From 50 m, the rock is relatively fresh but with slight oxidation and a faint greenish colouration. The greenish colouration intensity tends to increase with increasing depth. From a depth of 550 m, the trachyte is characterized by large phenocrysts of sanidine, set in a fine feldspar rich groundmass. Alteration varies at various depths ranging from moderate to high alteration in the middle to lower sections of the wells. Sanidine is completely altered to albite at these depths and high-temperature minerals of actinolite and wollastonite appear from 1366 m in Well MW-09 and 1858 m in Well MW-12 and persist to the bottom of the wells. Calcite is rare in this unit, especially from the surface to 800 m, but occurs where there are tuff intercalations, and the amount increases significantly at depths from 800 m to the bottom. Pyrite occurs intermittently from the depth of 700 m to the bottom of the wells.

Tuff: is encountered on several occasions in both wells, either as thick layers or lenses, intercalated with trachytes. Tuffs intersections are closely associated with both partial or total losses and high penetration rates. The first occurrence of a tuff layer in Well MW-09 was at 120 m, a 12 m thick layer immediately followed by a major loss zone. After the 200 m loss zone, tuff occurred as lenses intercalating with trachyte from 342 m to 428 m. Other thick tuff layers in this well were at 346-368, 510-536, 688-700, 742-780, 1438-1454, and at 1688-1700 m.

In Well MW-12, substantial layers of tuff were intercepted at 210-270, 328-354 and 400-434 m.

Syenite: A thin sheet of a syenitic intrusion was intercepted at 1948-1960 m in Well MW-09 and at 1872-2028 m in Well MW-12. It is whitish in colour, medium to coarse grained and porphyritic with dark greenish pyroxenes and amphiboles phenocrysts.

4.2.1 Lithology of Well MW-09

The lithology of Well MW-09 is shown in Figure 12.

0-2 m Pyroclastics: The formation contains a mixture of brownish tuff, pumice, trachyte, and obsidian.

2-14 m: Circulation loss.

14-16 m Trachyte: Grey, fine grained porphyritic trachyte.

16-24 m: Circulation loss.

24-28 m Trachyte: Grey to dark grey, fine grained porphyritic trachyte.

28-50 m Trachyte: Light grey, hypocrystalline trachyte with elongated phenocrysts of clinopyroxene.

50-72 m Trachyte: Light grey to brownish grey, fine grained, porphyritic trachyte. The formation is more oxidized than the overlying formation.

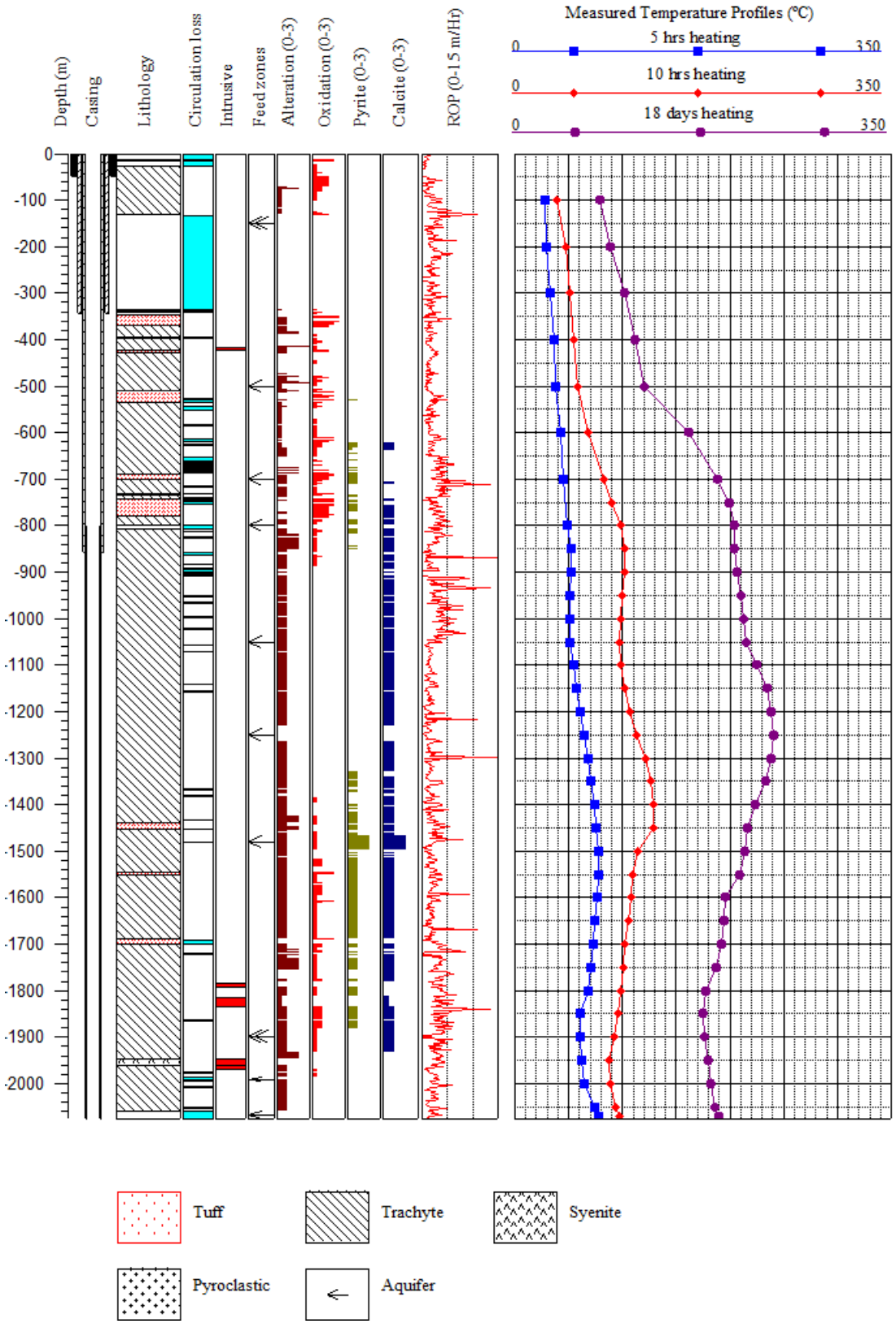

FIGURE 12: Lithology, alteration, ROP and temperature logs in Well MW-09

72-82 m Trachyte with tuff lenses: Light grey to greenish grey, fine grained trachyte. Few tuff fragments are observed at 76-82 m. The formation is fairly oxidized.

82-120 m Trachyte: Light grey to greenish grey, fine grained trachyte. The formations appear fresh but with a slight greenish coating.

120-132 m Tuff: Light grey, fine grained vesicular tuff. The vesicles are filled with amorphous silica and zeolites. The rock exhibits slight oxidation.

132-342 m: Circulation loss.

342-370 m Tuff: Brownish vesicular tuff with the vesicles being filled by amorphous silica and zeolites. The rock is slightly oxidized at the top and highly oxidized from 360-370 m. This unit is preceded by a major loss zone.

370-422 m Trachyte: Greenish grey fairly fresh, fine grained lava. It is porphyritic with phenocrysts of pyroxenes and feldspars. Pyrite is disseminated in the groundmass.

422-428 m Tuff: Reddish brown, fine grained vesicular rock unit with vesicles showing a silica lining. It is relatively oxidized. Fresh, fine grained trachyte grains were also observed.

428-510 m Trachyte: Light grey, fresh to greenish grey fine to medium grained rock, mainly composed of whitish feldspars and some pyroxenes. It is slightly altered to greenish clays. This unit exhibits some oxidation from 480-500 m.

510-526 m Tuff: Very light grey, fine grained rock that is fairly altered. The rock is vesicular with vesicles filled by silica. Reddish brown stains on the rock surface showed evidence of oxidation. Pyrite is disseminated in the groundmass. A few cuttings of trachyte were also noted at 526 m.

526-530 m: Circulation loss.

536-624 m Trachyte: Brownish grey, fine grained lava composed mainly of feldspars and pyroxene phenocrysts. The rock is altered. Occasional quartz veins are present. Pyrite is disseminated in the groundmass. Brownish grey lenses of fine grained tuff intercalations were observed between 536-552 m.

624-734 m Trachyte: Light grey fine, grained porphyritic lava composed of pyroxenes and large feldspar phenocrysts. The rock exhibits moderate oxidation and is slight alteration to light greenish clays. It contains a considerable amount of calcite and pyrite. Tuff lenses were observed within this unit, especially from 628-684 and 718-730 m. Intermittent losses were experienced at 624-628, 654-660, 684-684, 714-718, and 730-734 m.

734-780 m Tuff: Reddish brown, fine grained rock. It is vesicular at some instances with the vesicles being filled with calcite. Pyrite is disseminated in the groundmass. A few grains of trachyte were noted.

780-810 m Trachyte: Light grey, very fine grained, feldspar phyric trachyte. Some cuttings of brownish tuff were mixed with the trachyte. Losses were experienced at 784-790 m and 800-810 m.
810-864 m Trachyte: Grey to greenish grey, fine grained porphyritic rock with phenocrysts of feldspar and pyroxene. The rock is altered and has minor veins filled with quartz. Calcite also occurs as vesicle fillings. Pyrite is disseminated in the groundmass.

864-1300 m Trachyte: Light grey, medium grained feldspar porphyritic trachyte lava. Occasional phenocrysts of pyroxene are observed. The groundmass is almost 90% glassy. The rock exhibits slight alteration. Calcite is abundant across the unit and occurs as a vesicle infill. Pyrite was observed as disseminations on the groundmass and veinlet fillings from 810-854 m.

1300-1438 m Trachyte: Light grey to greenish grey, fine grained, porphyritic trachyte. This unit has abundant pyrite, chalcopyrite and calcite. High-temperature alteration minerals of actinolite and wollastonite appeared from1366 m.

1438-1448 m Tuff: Brownish to light greenish grey, fine grained tuff with sanidine in the matrix. Calcite, pyrite and chalcopyrite were noted in this unit.

1448-1468 m Trachyte: Light to yellowish/greenish grey, fine grained trachyte. The rock is highly altered. It has significant amounts of wollastonite.

1468-1548 m Trachyte: Grey to greenish and brownish grey, fine grained, porphyritic, highly altered trachyte. This unit has abundant pyrite, chalcopyrite, calcite and wollastonite.

1548-1552 m Tuff: Reddish brown, fine grained, vesicular tuff. The vesicles are filled with calcite and pyrite. Abundant pyrite was disseminated in the groundmass.

1552-1946 m Trachyte: Light grey to greenish grey, fine to medium grained feldspar phyric lava exhibiting slight alteration to green and brownish clays. Pyrite is notably abundant and disseminated on the surface of the rock fragments. Actinolite and wollastonite minerals were also observed in the rock unit. Minor tuff lenses were encountered at 1574-1596 m, 1674, 1712 m, and 1778-1782 m. The rock is highly altered.

1948-1960 m Syenitic intrusion: Whitish with dark green specs, fresh feldspar rich, coarse grained rock.

1960-2060 m Trachyte: Light grey to greenish grey, fine grained, highly altered trachyte mixed with bluish tuff fragments.

4.2.2 Lithology of Well MW-12

The lithology of Well MW-12 is shown in Figure 13.

0-12 m Pyroclastics: Mixed cuttings of reddish brown and light greenish grey, vesicular rock and volcanic glass.

12-16 m: Circulation loss.

16-166 m Trachyte: Grey, fine grained, relatively fresh, highly fractured trachyte.

166-270 m Tuff: Reddish brown to yellowish brown, highly oxidized, fine grained vesicular tuff. The vesicles are filled with amorphous silica. Loss of returns was experienced from 174-186, and 238-242 m.

270-332 m Trachyte: Grey to greenish grey, fine to medium grained, porphyritic trachyte. It consists of phenocrysts of mainly pyroxenes and feldspars. Circulation losses were experienced at 320-322 m.
332-354 m Tuff: Reddish brown, fine grained, vesicular tuff. The vesicle walls were lined with amorphous silica.

354-360 m: Circulation loss.

360-836 m Trachyte: Light to dark grey, fine to medium grained, porphyritic trachyte with minor tuff intercalations at 400, 412, 554, and 674 m. The rock contains feldspar and pyroxene phenocrysts. The main alteration minerals are chalcedony, calcite and pyrite. A significant amount of pyrite was noted at

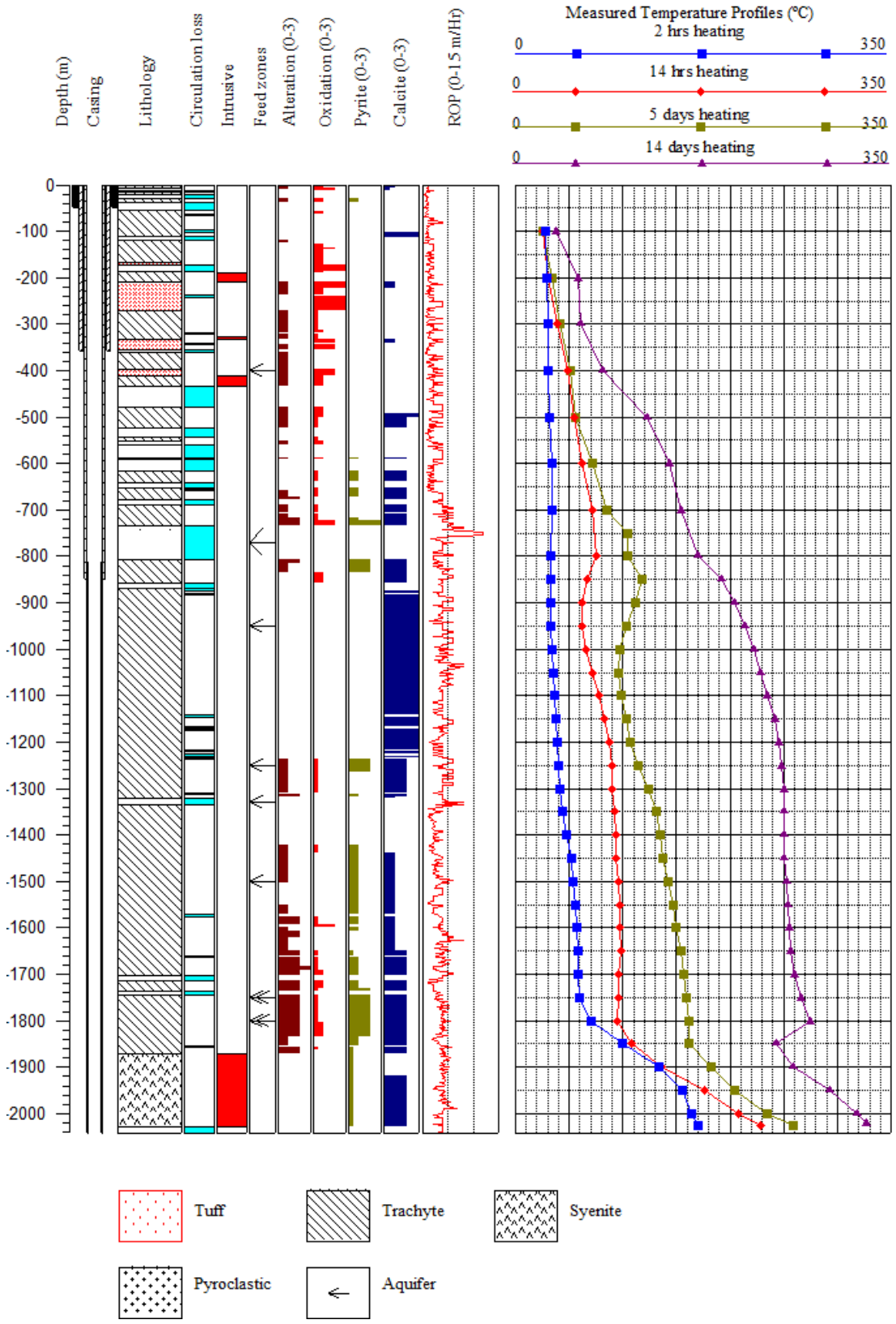

FIGURE 13: Lithology, alteration, ROP and temperature logs in Well MW-12

734 m. Calcite is present in this unit in varying extents. Major loss zones were encountered at 436-478, 562-588, 594-616, 642-652, 680-690, and 736-806 m.

836-1236 m Trachyte: Whitish, relatively fresh, medium to coarse grained porphyritic trachyte with phenocrysts of sanidine and occasionally augerine–augite. Calcite is abundant in this unit.

1236-1576 m Trachyte: Light grey to dark grey, fine to medium grained, porphyritic trachyte with large phenocrysts of sanidine and prismatic pyroxenes.

1576-1704 m Trachyte: Light grey to greenish grey, fine grained, porphyritic, moderately altered trachyte. Abundant pyrite was noted at 1594 m and 1600 m. The rock is intensely oxidized at 1600-1606 m. Chalcopyrite was noted from 1648-1704 m. The alteration intensity increases progressively with depth.

1704-1716 m: Circulation loss.

1716-1870 m Trachyte: Whitish to yellowish and greenish grey, fine grained highly altered trachyte. The rock shows abundant calcite and pyrite. Wollastonite appeared at 1858 m.

1870-2028 m Syenitic Intrusion: Light grey, coarse grained, massive and porphyritic syenite with large phenocrysts of sanidine and pyroxene. It exhibits low intensity of alteration and has abundant calcite.

4.3 Aquifers

In geothermal wells, faults and fractures in rocks enhance permeability. Geothermal wells are sited and drilled with the aim of intercepting high-temperature permeable zones. Aquifers in the Menengai wells were identified using temperature logs, hydrothermal alteration, circulation losses and the rates of penetration. Most of the permeable zones are associated with lithological contacts, characterized by intense oxidation and an abundance of calcite and pyrite. Possible locations of aquifers were identified in Well MW-09 at 150-350, 500, 700, 800, 1050, 1250, 1480, 1900, 1986-1996, and 2060-2077 m (Figure 12), summarized in Table 3.

TABLE 3: Inferred permeable zones in Well MW-09

Depth (m)	Evidence from geological observations, drilling observations and temperature monitoring profiles (logs)
150-350	Major circulation loss and increase in measured temperature
500	Lithological contact between tuff and trachyte, increase in measured temperature and oxidation intensity
700	Primary permeability in tuff, high oxidation intensity, abundance of pyrite, high rate of penetration
800	Circulation loss
1050	Increase in measured temperature
1250	Circulation loss, decrease (reversal) in measured temperature
1480	Lithological contact between tuff and trachyte, increase in alteration intensity, abundance of calcite and pyrite
1900	Fractured trachyte, increase in measured temperature
1986-1996	Circulation loss, increase in measured temperature
2060-2077	Circulation loss, increase in measured temperature

In Well MW-12, aquifers were encountered at 400, 740-800, 950, 1250, 1330, 1500, 1750, and 1800 m (Figure 13). The aquifers at 800 and 1350 m are associated with intense alteration and oxidation and preceded by circulation losses and high penetration rates. The aquifers at 1750 and 1850 m are the main feeders in the well and are associated with intrusive contacts. The host rock is intensely altered and oxidized and has abundant calcite and pyrite. Temperature measurements at this depth showed a sharp increase. Possible locations of aquifers in Well MW-12 are summarized in Table 4.

TABLE 4: Inferred permeable zones in Well MW-12

Depth (m)	Evidence from geological observations, drilling observations and temperature monitoring profiles (logs)
400	Primary permeability in tuff, increase in measured temperature
740-800	Major circulation zone, increase in rate of penetration, increase in measured temperature
950	Abundance of calcite, increase in measured temperature
1250	Fractured trachyte, increase in alteration intensity and oxidation, abundance of calcite and pyrite, increase in measured temperature
1330	Circulation loss, high penetration rate, increase in measured temperature
1500	Increase in measured temperature, increase in rate of penetration, abundance of pyrite and calcite
1750	Sharp increase in measured temperature, intense alteration, abundant pyrite and calcite
1850	Sharp temperature kick, high-alteration intensity, abundant calcite and pyrite, oxidation

5. ALTERATION AND HYDROTHERMAL MINERALOGY

5.1 Primary minerals

The primary minerals are rock forming minerals that were formed during the crystallisation of magma as it cooled. These minerals become unstable when subjected to hydrothermal conditions and are replaced by secondary minerals which are stable at the new temperatures and pressure conditions (Browne, 1978). The primary minerals observed in rock cuttings from Wells MW-09 and MW-12 includes: volcanic glass, pyroxene, olivine, amphibole, feldspar, and Fe-Ti oxides. As these minerals were exposed to alteration, they were subsequently replaced by several secondary minerals. A summary of the primary minerals and their corresponding secondary products is given in Table 5.

TABLE 5: Primary minerals and their secondary alteration products (modified from Browne, 1982)

Primary minerals	Secondary mineral products
Volcanic glass, quartz, amorphous silica	Zeolites, quartz, clays, calcite
Olivine	Clays
Pyroxene, amphibole	Clays, pyrite, calcite, actinolite
Sanidine	Calcite, clay, albite
Fe-Ti oxide	Pyrite, sphene

Volcanic glass: Volcanic glass is common in the near surface formations in Wells MW-09 and MW-12. It is formed by the quenching of magma to form glassy obsidian fragments. They exhibit conchoidal fracturing and frequently have brownish tints of oxides.

Olivine: Olivine is rare in both wells and occurs as greenish glassy crystals. It is identified by its poor/lack of cleavage and high birefringence under the petrographic microscope. It alters to clays.

Pyroxene: These are relatively abundant in trachyte but rare in syenite and tuff in both wells. They are clearly identified in binocular microscope as dark prismatic minerals and by their near right angle (87º/93º) cleavage. These minerals exhibit little alteration near the surface but the intensity of alteration increases with depth. The pyroxenes mainly alter to amphiboles and actinolite at depth. The main type of pyroxene observed was augerine-augite.

Amphiboles: Amphiboles are identified by their strong pleochroism and perfect cleavage at 124º/56º under the petrographic microscope. They exhibit little alteration near the surface but the intensity of alteration increases with depth where they mainly alter to clays.

Sanidine: This is the main type of phenocryst found in Wells MW-09 and MW-12, easily identified using binocular and petrographic analyses. They alter to calcite, clays and albite at depth. When viewed under petrographic microscope, it is colourless in plane polarized light and grey in crossed polarized light. It is characterized by its distinctive Carlsbad twinning.

Fe-Ti Oxides: The most abundant opaques in the wells and are relatively resistant to alteration. These oxides occur as magnetite and mostly alter to sphene.

5.2 Hydrothermal minerals

Hydrothermal minerals in Menengai occur as replacements of primary minerals or as vein and vesicle fillings. Permeability and porosity of the rocks control the access of thermal fluids, which results in hydrothermal alteration of the rocks and precipitation of secondary minerals in open spaces (Lagat, 2004). Most of the hydrothermal minerals were identified by binocular analysis and subsequently confirmed using petrographic analysis. The main hydrothermal alteration minerals and their distribution in Wells MW-09 and MW-12 are shown in Figures 14 and 15 and are described below:

Zeolites are rare in both wells. The zeolite types identified were scolecite and mesolite. They occur as densely packed fibrous aggregates often radiating from several sources along vesicle walls, especially in tuff layers. Zeolites are generally thermodynamically metastable at 60-110 °C (Kristmannsdóttir, 1979). The first occurrence of zeolites in Well MW-12 was close to the surface. They also occurred at 8.82 and 402 m. In Well MW-09, they were only encountered at 82 and 122 m.

Pyrite is found in abundance in both wells. It was observed from 530-850 and 1350-1880 m in Well MW-09 and at 600-840, 1240-1260 m and from 1420 m to the bottom of Well MW-12. It occurs as cubic crystals with brassy yellow lustre in reflected light. It is mainly observed as fine disseminations and as large cubic crystals in the feldspathic groundmass in trachytes and to a lesser extent as deposits in fractures, vesicles and veins. Abundance of pyrite indicates good permeability (Lagat, 2008; Reyes, 2000). This is evident in both wells, where most of the inferred aquifers were characterized by an abundance of pyrite.

Chalcopyrite was observed from 400-500 and 1350 m to the bottom of Well MW-09 and 1650-1850 m in Well MW-12. It occurs as fine disseminations in the rock and as deposits in veinlets. It is distinguished from pyrite by a golden tinge to bronze colour and tetragonal crystal symmetry.

Albite occurs as an alteration mineral of sanidine feldspar. Albite alteration was observed under petrographic microscope from 660 m in Well MW-12 and 1860 m in Well MW-09 to the bottom of well columns. They indicate temperatures of above 180ºC (Kristmannsdóttir, 1979) and appear as dirt on the surface of the sanidine feldspars.

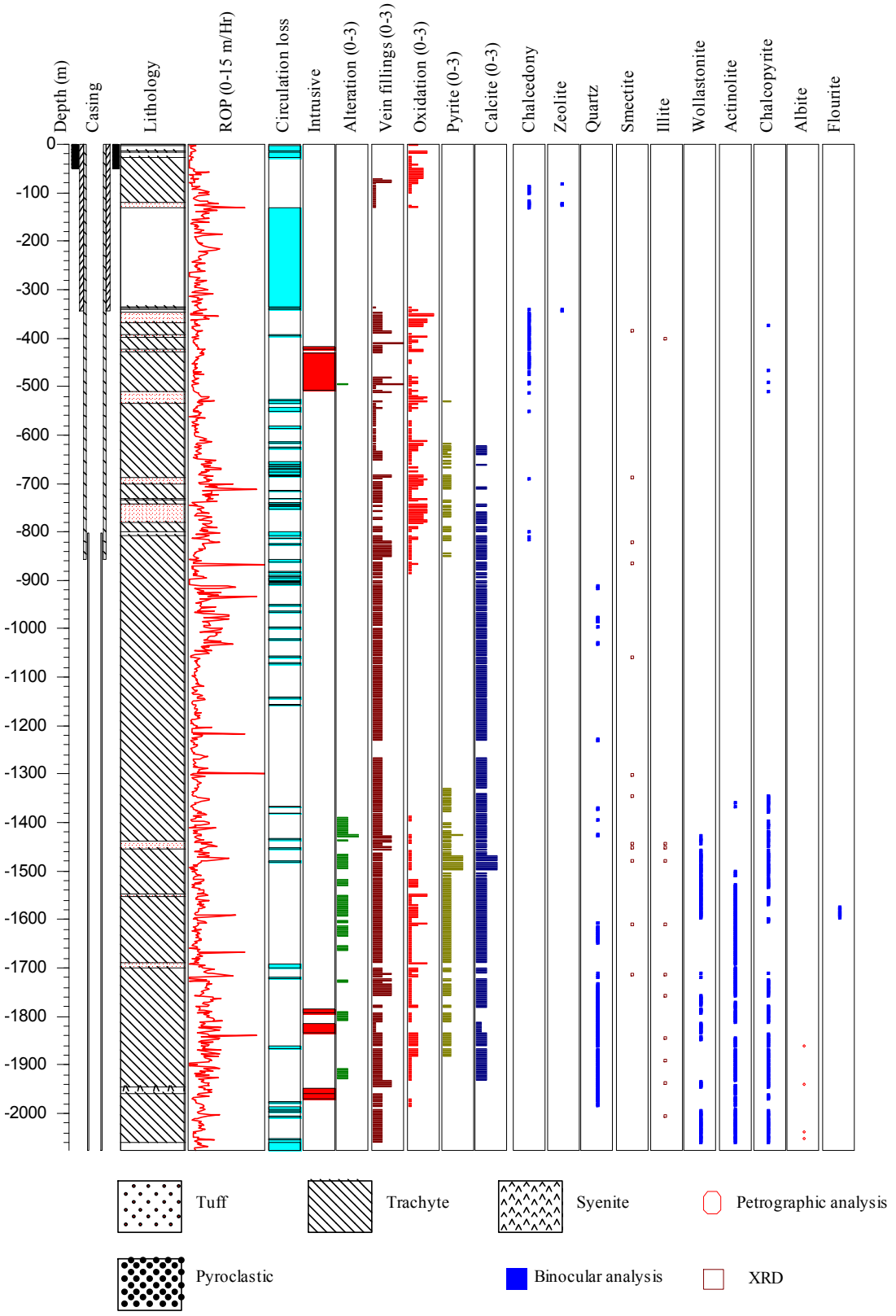

FIGURE 14: Alteration minerals and their distribution in Well MW-09

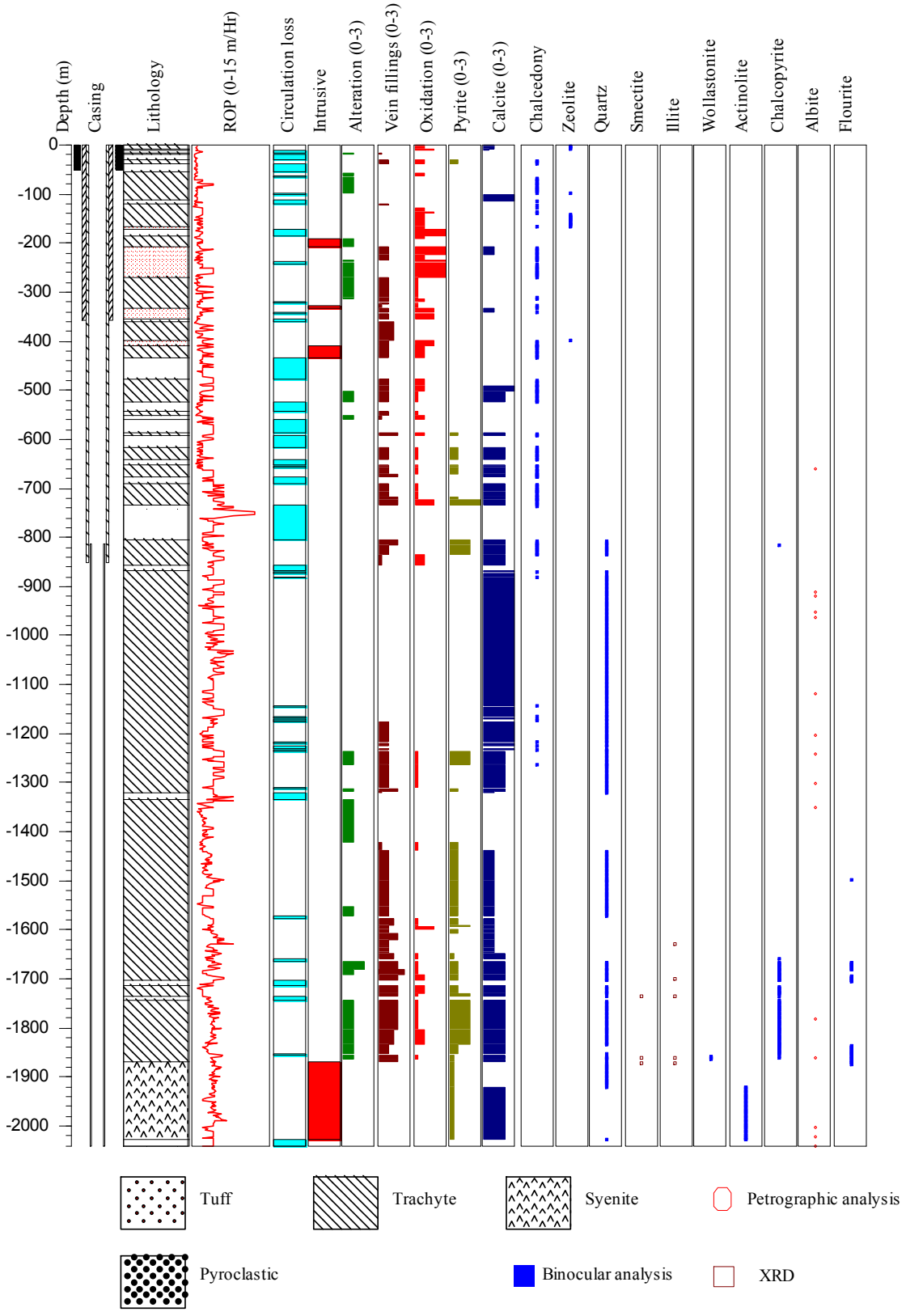

FIGURE 15: Alteration minerals and their distribution in Well MW-12

Opal occurs at shallow depths as a white or milky white lining in vesicles and veins, especially in the tuffs. Opal is a low-temperature silica mineral that is stable at temperatures between 20-100°C. In Well MW-09, it occurred from 86-130 m while in Well MW-12, it occurred from 32-226 m.

Chalcedony occurs intermittently in the wells, often as colourless to whitish globules on rock surfaces and as linings in vesicles and veins. It was observed from 126-800 m in Well MW-09 and from 226-1260 m in Well MW-12. Its presence indicates temperatures of above 100ºC (Kristmannsdóttir, 1979). At depths where the formation temperature exceeds 180°C, chalcedony is replaced by quartz (Lagat, 1995).

Calcite occurs intermittently in varying amounts distributed down the well columns. In Well MW-09 it occurred from 512 m to 1992 m, where it disappeared. Calcite is stable at temperatures below 300°C and, therefore, its disappearance at 1992 m may signify temperatures exceeding 300°C below that depth. In Well MW-12, calcite occurred from the surface to the bottom of the well. The mineral occurs in vesicles, veins and disseminated in the groundmass where it replaces sanidine feldspar. Calcite presence is associated with carbon dioxide activity in the reservoir.

Oxides are mainly noted in the wells at shallow depths and where water interacts with the rocks. The most common ones are iron oxides. In both wells, oxidation occurrence was noted from the surface to around 900 m depth and from 1250 to 1900 m.

Quartz: Secondary quartz started to appear at 900 m and 800 m in Wells MW-09 and MW-12, respectively, and persisted almost to the bottom of both wells. At shallow depths, it occurs as a replacement product of chalcedony while at deeper depth it is deposited in veins and vesicles. Quartz is colourless to white in colour, and occurs as euhedral to subhedral crystals. It is easily recognized in petrographic analysis by its low relief, low birefringence and lack of cleavage or twinning. The presence of secondary quartz below 900 m depth indicates that the formation temperature is more than 180°C.

Wollastonite is a colourless, fibrous mineral when viewed both under the binocular and petrographic microscopes. It occurred from 1426 m depth to the bottom of Well in MW-09 and from 1858 m to 1864 m in Well MW-12. The presence of wollastonite is indicative of formation temperatures higher than 270°C (e.g. Njue, 2010).

Actinolite forms in close association with wollastonite. Actinolite appeared at 1508 m in Well MW-09 and at 1922 m in Well MW-12. It is green to greyish green in colour and grows as fibrous prismatic crystals. The mineral is formed as a replacement of pyroxene. The presence of actinolite is associated with temperatures exceeding 280ºC (Reyes, 2000).

*Clay mineral*s are alteration products of primary rock forming minerals. The type of clay formed depends on the temperature, fluid composition, pH and the permeability of the formation. Clay minerals are rare in Wells MW-09 and MW-12. Two types of clay minerals were identified by the use of the X-ray diffraction analysis (XRD). The clays encountered were:

Smectite occurred at 386 m and from 688-1714 m in Well MW-09. They displayed high peak values of 12.2-13.6 Å in untreated and 12.9-14 Å in glycolated samples and 10 Å when heated. In Well MW-12, smectite occurred from 1736 m and persisted to the bottom of the well. It displayed values of 12.8-17.7 Å in both untreated and glycolated samples, and 10.3 Å in the heated sample. The occurrence of smectites indicates temperatures lower than 200°C.

Illite forms at temperatures above 200°C. In Well MW-09, illite occurred at 400 m and from 1444 m to the bottom of the well. It displayed peaks between 10.3 Å in untreated, glycolated and heated samples. In Well MW-12, it occurred at 1630 m and from 1700 m to the bottom of the well.

5.3 Alteration mineral zonation

Based on the clay XRD, binocular and petrographic analysis of samples from Wells MW-09 and MW-12, an alteration mineral zonation model could be constructed. The main minerals used were zeolites, chalcedony, quartz, actinolite, wollastonite and clays. Clay minerals are very useful for the interpretation of thermal history of a geothermal system because of their quick response to temperature change (Kristmannsdóttir, 1979). From the hydrothermal mineral assemblages, three major alteration zones were identified in Wells MW-09 and MW-12 below an unaltered zone (Figure 16). The zones are:

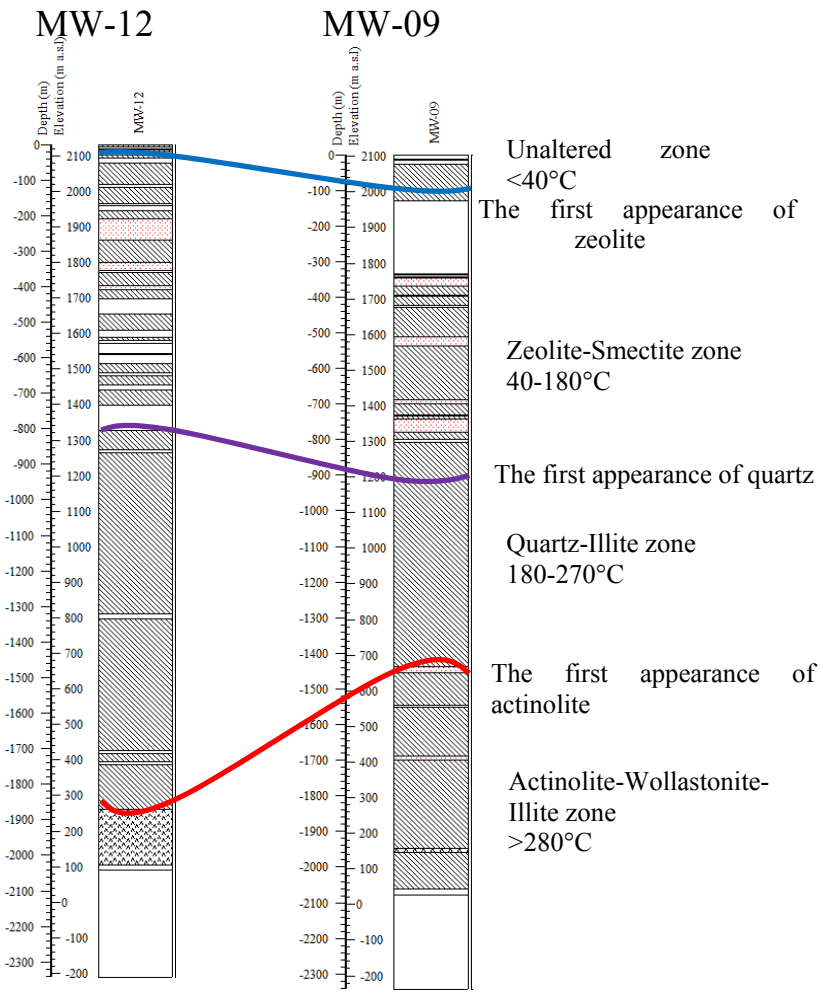

FIGURE 16: Alteration mineral zonation profile in Wells MW-09 and MW-12

Unaltered zone: The top 50-80 m of both wells is characterized by low alteration. The rocks are generally fresh but oxidation is due to interaction with the surface and cold groundwater.

Smectite-Zeolite zone: This zone is characterized by the first appearance of zeolites and chalcedony and the presence of low-temperature smectite clay. Zeolites and chalcedony were identified by binocular and petrographic microscopes while smectite was confirmed by XRD analysis. This mineralogical assemblage represents temperatures below 180°C.

Quartz-Illite zone: This zone is marked by the first appearance of quartz and the presence of high-temperature clays (illite). The mineralogical assemblage indicates temperatures of above 180°C.

Actinolite-Wollastonite-Illite zone: This zone is characterized by the first appearance of wollastonite and actinolite and the presence of illite. The occurrence of actinolite suggests formation temperatures of above 280°C (Reyes, 2000), and was seen from 1400 m in Well MW-09 and 1900 m in Well MW-12.

5.4 Fluid inclusion geothermometry

Fluid inclusion geothermometry is a powerful tool for outlining changes in temperature regimes in a geothermal system. Fluid inclusions are tiny bubbles of liquid and vapour that are formed when fluids are trapped in crystals and subsequently cooled due to differential thermal contraction of fluid and host

mineral. Primary inclusions are formed during primary crystal growth, often concentrated along the first order of growth discontinuity or occur as isolated inclusions distributed within the crystal (Roedder, 1984). Secondary inclusions are formed after primary growth, often along healed micro-structures. The inclusions trapped in minerals during crystallization or recrystallization were analysed to determine the temperature at which the inclusions/vacuoles were formed.

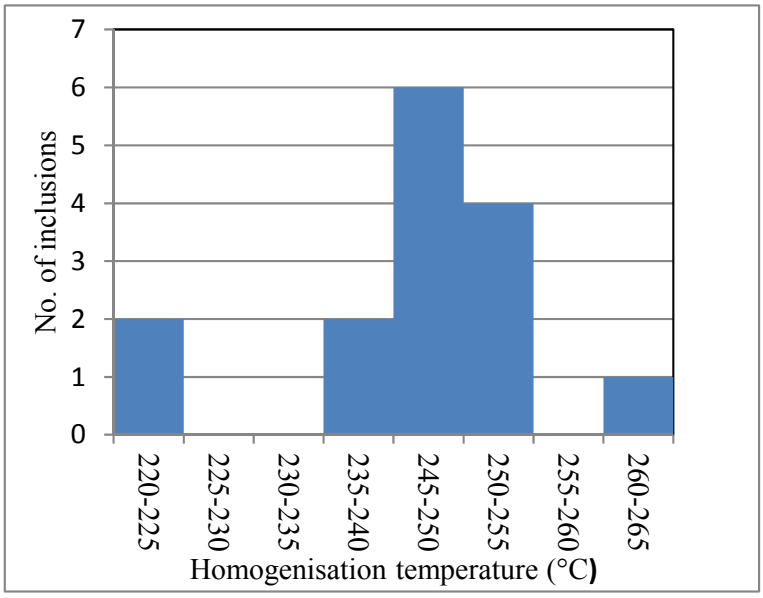

FIGURE 17: Fluid inclusion measurements from a calcite crystal at 1000-1100 m in Well MW-09

Mineral crystals from selected depth ranges from both wells were picked for fluid inclusion analysis. They were heated using a Linkam THSMG 94 stage and the temperatures at which the inclusions reached homogenisation temperature and the bubbles disappeared were noted. The temperature measurements were recorded at 5°C intervals. The temperatures at which the bubbles disappeared correspond to the temperatures at which the fluids were trapped in the crystal. This is referred to as the homogenisation temperature (T_h). A calcite crystal from 1000-1100 m depth range in Well MW-09 and a quartz crystal from 874-884 m in Well MW-12 were used for the analysis of fluid inclusions and their temperatures of homogenisation were recorded. The homogenisation temperature values of fifteen fluid inclusions in a calcite crystal from Well MW-09 ranged from 220 to 260ºC with an average of 245°C (Figure 17). Twenty nine fluid inclusions were identified and studied in a quartz crystal from Well MW-12. The homogenisation temperature values in the inclusions ranged from 250-345°C, with an average value of 300°C (Figure 18).

Correlations were made between measured temperatures, hydrothermal alteration temperatures, boiling depth curves, and fluid inclusion temperatures in both wells, presented in Figures 19 and 20. From the data, it is difficult to interpret whether the wells are in equilibrium or heating up. In Well MW-09, the alteration, measured and fluid inclusion temperatures plot within the same range from 210-245°C. The temperature measurements used in the comparison shown in

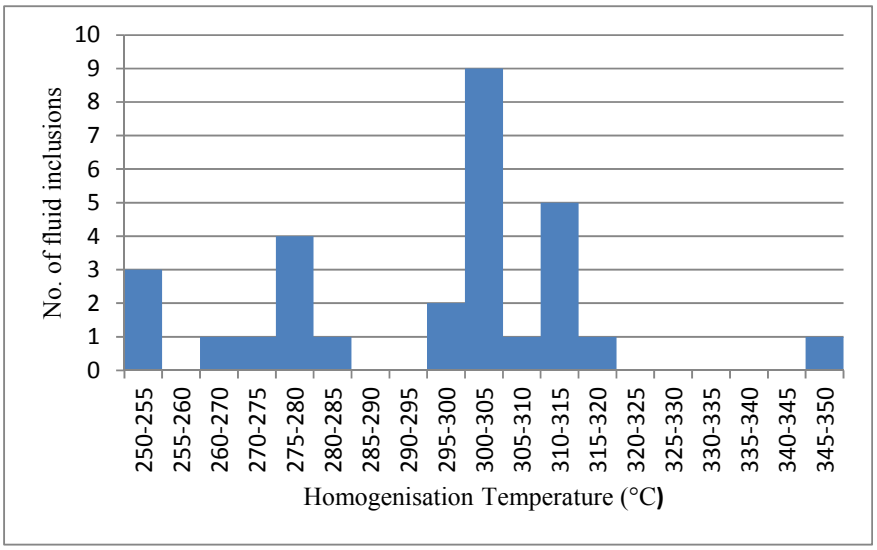

FIGURE 18: Fluid inclusion measurements from a quartz crystal from 874-884 m depth range in Well MW-12

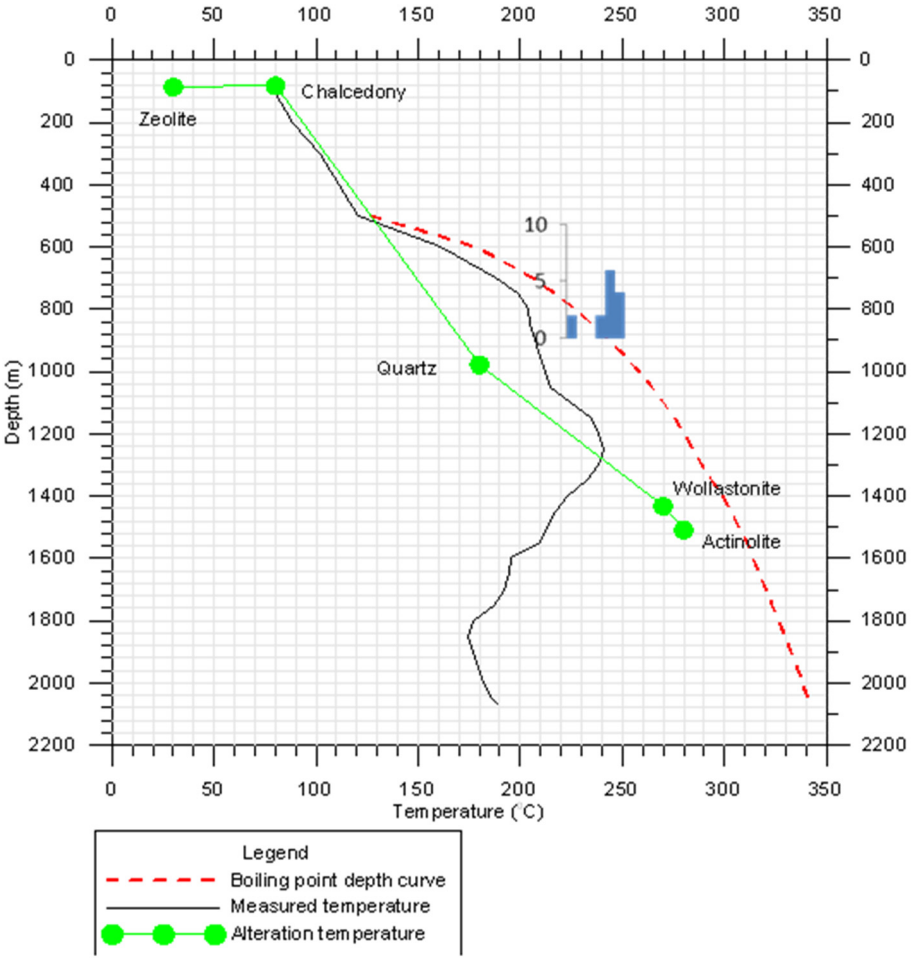

FIGURE 19: Comparison between fluid inclusion temperature, alteration temperature, measured temperature and the calculated boiling point depth curve in Well MW-09

Figure 19 were taken after 18 days of heating. The measured temperature, however, does not reflect the formation temperature after such a short time of heating up, i.e. the well has not yet recovered. The temperatures varied significantly in Well MW-12. At 880 m, the depth from where the quartz crystal for fluid inclusions was picked, the average homogenisation temperature is 300°C while the alteration temperature is 190°C and the measured temperature is 210°C. The temperature measurements plotted, were taken after 14 days of heating. Fluid inclusion temperatures in both wells, plotted along the boiling point depth curve and, therefore, represent boiling conditions. However, the measured well temperatures were generally higher than the alteration temperatures, and are still rising, indicating that the wells are heating up.

6. DISCUSSION

Menengai is located at the centre of the Kenya dome which is experiencing crustal thinning caused by a mantle plume. Tectonically, the central volcano is set at a triple junction where the Nyanza Rift branches from the main rift and developed on a potential tail-crack end structure at the southern end of the complex N-S striking Solai TVA (Chorowicz, 2005). A NNW-SSE trending ridge that is part of Molo TVA is believed to cut through the caldera. All of these structures play an important role in enhancing permeability in Menengai.

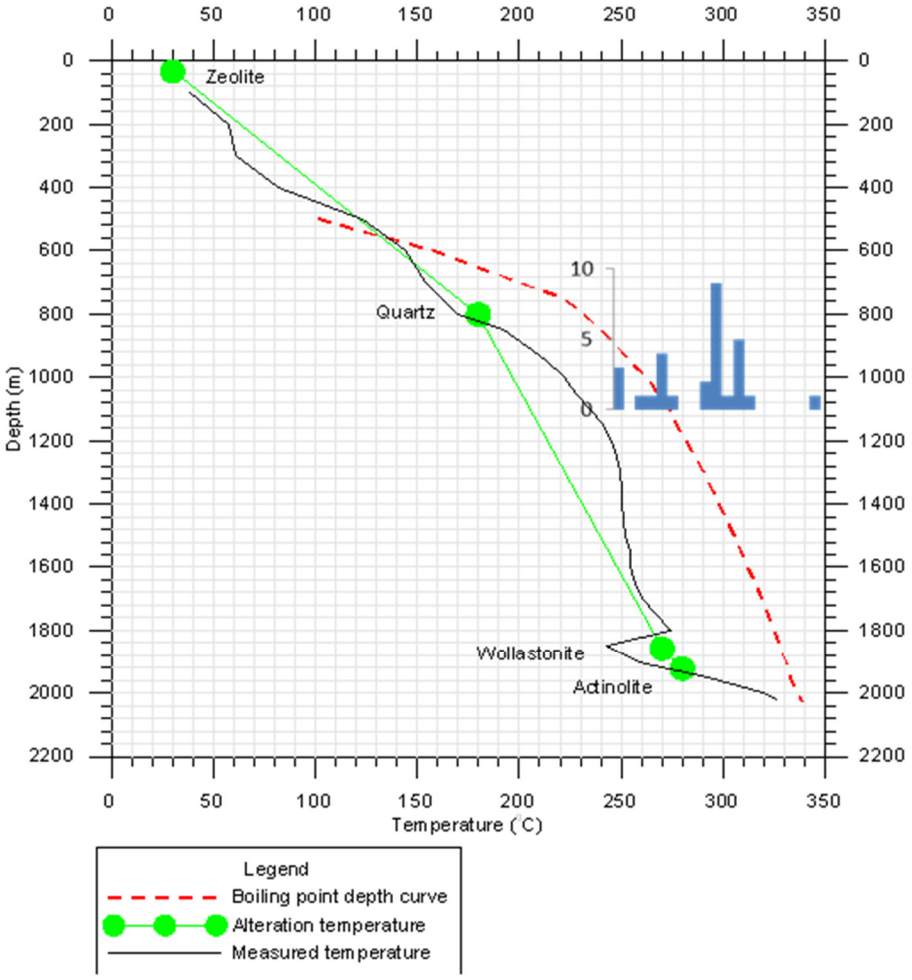

FIGURE 20: Comparison between fluid inclusion temperature, alteration temperature, measured temperature and the calculated boiling point depth curve in Well MW-12

The litho-stratigraphic units of Wells MW-09 and MW-12 generally show close similarity to the other wells previously drilled within the Menengai caldera (Omondi, 2011; Mibei, 2012; Kipchumba, 2013). The upper sections of the wells consist of a thin layer of pyroclastics underlain by a 50-80 m layer of blocky unconsolidated recent trachyte lavas and 100-200 m thick massive trachyte lavas. These form the post-caldera lavas erupted within the caldera. Thick tuff layers were encountered at 342-368 m in Well MW-09 and somewhat shallower, at 210-270 m, in Well MW-12. However, the tuff layer in Well MW-09 is probably shallower and thicker than indicated, as a major circulation zone preceded its occurrence. The tuff layer marks a boundary between the post-caldera and pre-caldera volcanics and cuts across all the other wells previously drilled in Menengai and is, therefore, an important marker horizon. Major circulation losses occurred either before or after the tuff layer and in some instances within the tuff layer. The middle sections of the wells mainly consist of trachyte lavas with occasional tuff intercalation.

The hydrothermal mineral distribution in both wells showed progressive temperature increase with depth. The analyses of sample cuttings indicate that low-temperature minerals like zeolites, chalcedony and low-temperature clays, dominate the upper sections of the wells. Moderately high to high-temperature hydrothermal minerals, ranging from 180 to >300ºC, were encountered from the mid to the lower sections of the wells, based on the occurrence of secondary quartz, albite, wollastonite and actinolite. The abundance of pyrite and chalcopyrite signify that the wells are highly permeable. The hydrothermal mineralogy generally indicates that the wells are located in a high-temperature geothermal system.

The comparison between lithologic sequences across Wells MW-12, MW-09, MW-08 and MW-11 shows close similarities, but displays relative vertical displacements (Figure 21). The circulation losses experienced at the presumed tuff marker horizon associated with the caldera collapse makes stratigraphic correlations difficult.

Homogenisation fluid inclusion temperatures, measured temperatures and alteration temperatures indicate that the system may be in equilibrium or more likely, to be heating up. Fluid inclusion temperatures in both wells plot along the boiling point depth curve and, therefore, represent boiling conditions in the wells. However, correlation between measured and alteration temperatures, which represents the current condition, indicate that the wells may be heating up.

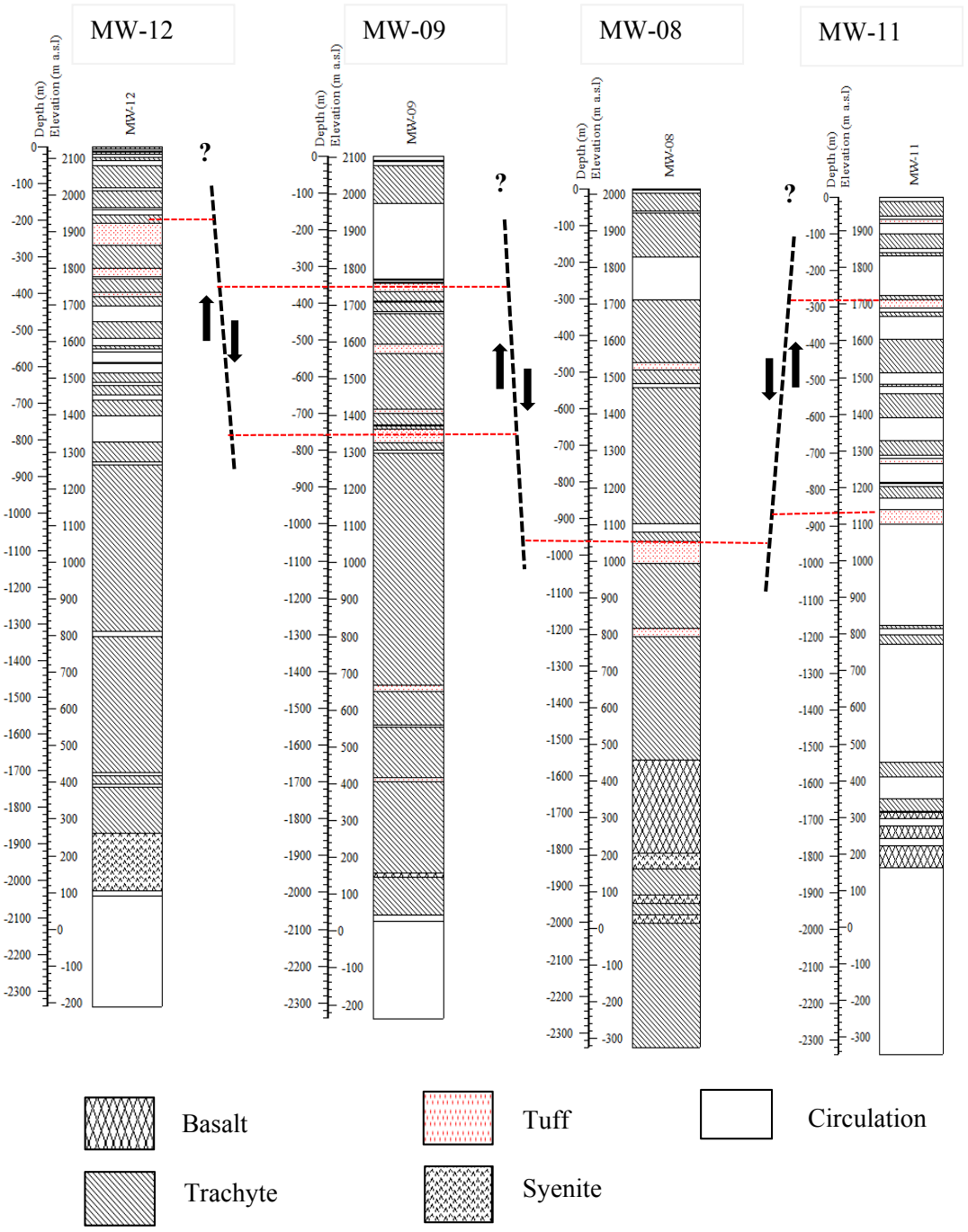

FIGURE 21: Stratigraphic correlation of Wells MW-12, MW-09, MW-08 and MW-11 (MW-08 and MW-11 from Kipchumba, 2013)

7. CONCLUSIONS AND RECOMMENDATIONS

1. Regional and local tectonics play an important role in enhancing permeability in Menengai geothermal system. Post-caldera lava flows issued from a postulated tail-crack structure that developed west of the N-S striking zone of normal faults has a dextral strike-slip throw component (Solai TVA).

2. The lithostratigraphy of Menengai wells is predominantly composed of trachytes and tuff layers.

3. Several aquifers were identified in Wells MW-09 and MW-12, based on temperature logs, hydrothermal alteration, circulation losses and the rates of penetration. Sources of permeability in the wells are fractures and faults, lithological contacts and primary permeability of tuffs.

4. Based on hydrothermal minerals assemblages, three alteration zones were defined below a zone free of alteration. These are: smectite-zeolite zone, quartz-illite zone and actinolite-wollastonite-illite zone.

5. The abundance of pyrite and chalcopyrite signifies that the wells are highly permeable. The permeable zones were also characterized by high alteration intensity and oxidation, especially at lithological contacts and high penetration rates.

6. The measured temperature logs do not reflect the true formation temperature since the wells had not recovered when the available temperature logs were taken. More temperature measurements should be carried to ascertain the recovery.

7. Results from fluid inclusion measurements are preliminary and relatively inconclusive. Therefore, further fluid inclusion analyses should be carried out, particularly at deeper levels in the wells.

ACKNOWLEDGEMENTS

I wish to express my sincere gratitude to the Government of Iceland and the United Nations University (UNU), for granting me a fellowship to undertake specialized training at the UNU-Geothermal Training Programme. Special thanks to Mr. Lúdvík S. Georgsson, the director, and Dr. Ingvar B. Fridleifsson, former Director, of UNU-GTP. I wish to acknowledge my employer, the Geothermal Development Company (GDC) for granting me permission to attend the course. I'm deeply indebted to my supervisors, Dr. Hjalti Franzson, Dr. Björn S. Hardarson and Ms. Anette K. Mortensen for their indispensable assistance and guidance in my project. To the Iceland GeoSurvey (ISOR) staff and all the lecturers, thank you so much for sharing your skills and knowledge. To the UNU-GTP staff, Ms. Thórhildur Ísberg, Mr. Markús A.G. Wilde, Mr. Ingimar G.Haraldson, and Ms. Málfrídur Ómarsdóttir, thank you for your invaluable support during my stay in Iceland.

Special thanks to my wife, Eglah, my daughter, Cherop and my son, Ruto and the entire family for prayers, encouragement, support and for enduring my long absence.

I thank God for his sufficient grace, endless love and care.

REFERENCES

Baker, B.H., and Wohlenberg, J., 1971: Structural evolution of the Kenya Rift Valley. *Nature, 229*, 538-542.

Baker, B.H, Mohr, P.A, and Williams, L.A.J., 1972: Geology of the Eastern Rift System of Africa. *Geological Society of America, Special Paper 136,* 1-67.

Baker, B.H., Williams, L.A.J., Miller, J.A., and Fitch, F.J., 1971: Sequence and geochronology of the Kenya Rift volcanics. *Tectonophysics, 11*, 191-215.

Browne, P.R.L., 1978: Hydrothermal alteration in active geothermal fields. *Annual Review Earth & Planetary Sciences,* 6, 229-250.

Browne, P.R.L., 1982: Permeability in geothermal fields and hydrothermal alteration. In: Hochstein, M.P. (ed.), *Introduction to geothermal prospecting*. Auckland University, Auchland, NZ, 50-54, and 85-89.

Burke K., and Dewey J., F. 1973: Plume generated triple junctions: Key indicators in applying plate tectonics to old rocks. *J. Geol., 81*, 406-433.

Chorowicz, J., 2005: The mechanisms of the East African Rift System formation. *J. African Earth Science, 43*, 379-410.

Ebinger, C. J., and Sleep, N. H., 1998: Cenozoic magmatism throughout east Africa resulting from impact of a single plume. *Nature, 365*, 788-791.

GDC, 2010: *Menengai geothermal prospect, an investigation for its geothermal potential*. GDC, Nakuru, Kenya, Geothermal Resource Assessment Project, internal report, 66 pp.

George, R.M.M., Rogers, N.W., and Kelley, S., 1998: Earliest magmatism in Ethiopia: evidence for two plumes in one flood basalts province. *Geology, 26*, 923-926.

Geotermica Italiana Srl., 1987: *Geothermal reconnaissance survey in the Menengai - Bogoria area of the Kenya Rift Valley*. UN (DTCD)/GOK, report.

Gichira, J.M., 2012: Joint 1D inversion of MT and TEM data from Menengai geothermal field, Kenya. Report 11 in: *Geothermal training in Iceland 2012*. UNU-GTP, Iceland, 137-167.

KenGen, 2004: *Menengai volcano: Investigations for its geothermal potential*. KenGen and Ministry of Energy, Geothermal Resource Assessment Project, internal report.

Kipchumba, J. L., 2013: Borehole geology and hydrothermal alteration of wells MW-08 and MW-11, Menengai geothermal field, Kenya. Report 10 in: *Geothermal training in Iceland 2013*. UNU-GTP, Iceland, 37.

Korme, T., Chorowicz, J., Collet, B., and Bonavia, F.F., 1997: Volcanic vents rooted on extension fractures and their geodynamic implications in the Ethiopian Rift. *J. Volcanology & Geothermal Res., 79,* 205–222.

KRISP Working Group, 1987: Structure of The Kenya Rift from seismic refraction. *Nature, 325*, 239-242.

Kristmannsdóttir, H., 1979: Alteration of basaltic rocks by hydrothermal activity at 100-300°C. In: Mortland, M.M., and Farmer, V.C. (editors), *International Clay Conference 1978*. Elsevier Scientific Publishing Co., Amsterdam, 359-367.

Lagat, J.K., 1995: Borehole geology and hydrothermal alteration of well OW-30, Olkaria geothermal field, Kenya. Report 6 in: *Geothermal Training in Iceland 1995,* UNU-GTP, Iceland, 135-154.

Lagat, J.K., 2004: *Geology, hydrothermal alteration and fluid inclusion studies of the Olkaria Domes geothermal field, Kenya.* University of Iceland, MSc thesis, UNU-GTP, Iceland, report 2, 71 pp.

Lagat, J.K., Arnórsson, S., Franzson, H., 2005: Geology, hydrothermal alteration and fluid inclusion studies of Olkaria Domes geothermal field, Kenya. *Proceedings of the World Geothermal Congress 2005, Antalya, Turkey*, 14 pp

Leat, P. T., 1984. Geological evolution of the trachytic caldera volcano Menengai, Kenya. *J. Geol. Soc. London*, *141*, 1057-1069.

MacDonald, R., and Scaillet, B., 2006: The central Kenya peralkaline province: insights into the evolution of peralkaline salic magmas. *Lithos, 91*, 59-73.

MacDonald, R., Bailey, D. K., and Sutherland, D., 1970: Oversaturated peralkaline glassy trachyte from Kenya. *J. Petrology, 11*, 507-517.

MacDonald, R., Black, S., Fitton, J. G., Rogers, N. W., and Smith, M., 2001: Plume-lithospheric interactions in the generation of the basalts of the Kenya Rift, East Africa. *J. Petrology, 42,* 877-900.

Mechie, J., Keller, G.R., Prodehl, C., Khan, M.A., and Gaciri, S.J., 1997: A model for the structure, composition and evolution of the Kenya rift. *Tectonophysics, 278*, 95-119.

Mibei, G., 2012: Geology and hydrothermal alteration of Menengai geothermal field. Case study: wells MW-04 and MW-05. Report 21 in: *Geothermal training in Iceland 2012*. UNU-GTP, Iceland, 437-465.

Njue, L.M., 2010: Borehole geology and hydrothermal mineralisation of well HE-27, Hellisheidi geothermal field, SW-Iceland. Report 24 in: *Geothermal training in Iceland 2010*. UNU-GTP, Iceland, 463-492.

Omondi, C., 2011: Borehole geology and hydrothermal mineralisation of wells MW-01 and MW-02, Menengai geothermal field, Central Kenya Rift Valley. Report 30 in: *Geothermal training in Iceland 2011*. UNU-GTP, Iceland, 737-773.

Reyes, A.G., 2000: *Petrology and mineral alteration in hydrothermal systems. From diagenesis to volcanic catastrophes*. UNU-GTP, Iceland, report 18-1998, 77 pp.

Roedder, E., 1984: *Fluid inclusions*. Mineral. Soc. Am., Rev. Mineral., 12, Washington, DC, 644 pp.

Rogers, N., Macdonald. R., Fitton, J.G., George, R., Smith, M., Barreiro, B., 2000: Two mantle plumes beneath the East African rift system: Sr, Nd and Pb isotope evidence from Kenya Rift basalts. *Earth & Planet. Science Letters, 176*, 387-400.

Simiyu, S.M., 2010: Application of micro-seismic methods to geothermal Exploration: Examples from the Kenya rift. *Paper presented at "Short Course V on Exploration for Geothermal Resources", organized by UNU-GTP, GDC and KenGen, at Lake Bogoria and Lake Naivasha, Kenya,* 27 pp.

Simiyu, S.M., and Keller, G.R., 1997: Integrated geophysical analysis of the East African Plateau from gravity anomalies and recent seismic studies. *Tectonophysics, 278,* 291-314.

Smith, M., 1994: Stratigraphic and structural constraints on mechanisms of active rifting in the Gregory Rift, Kenya. *Tectonophysics, 236*, 3-22.

Smith, M., and Mosley, P., 1993: Crustal heterogeneity and basement influence on the development of the Kenya Rift, East Africa. *Tectonics, 12*, 591-606.

APPENDIX I: Results of the XRD analysis for Well MW-09

Depth (m)	D(001) Untreated	D(001) Glycolated	D(001) Heated	Mineral	Type	Other minerals
76				No clay		8,6Å
386	~13.6	~13.6	Destroyed	Sm:sm	Smectite	Amphibole
400	10.3	10.3	10.3	Illite	Illite	Amphibole
482				No clay		Amphibole
512				No clay		Amphibole
636				No clay		
688	12.9	>12.9	~10	Sm:sm	Smectite	
820	13.6	14	10.2	Sm:sm	Smectite	
864	13.5	>13.5	~10	Sm:sm	Smectite	
1060	13.5	>13.5	~10	Sm:sm	Smectite	
1302	13.5	>13.5	~10	Sm:sm	Smectite	Amphibole
1344	13.5	>13.5	~10	Sm:sm	Smectite	Amphibole
1388				No clay		
1424				No clay		
1436				No clay		
1444	12.2/10	>12.2/10	~10	Sm: sm/ill	Smectite-Illite	Amphibole
1452	12.2/10	>12.2/10	~10	Sm: sm/ill	Smectite-Illite	Amphibole
1478	12.2/10	>12.2/10	~10	Sm: sm/ill	Smectite-Illite	Amphibole
1610	12.2/10	>12.2/10	~10	Sm: sm/ill	Smectite-Illite	Amphibole
1684				No clay		
1714	14.1/10.3	14.1/10.3	10.3	Sm: sm/ill	Smectite-Illite	Amphibole
1756	10.3	10.3	10.3	Illite	Illite	Amphibole
1844	10.3	10.3	10.3	Illite	Illite	Amphibole
1890	10.3	10.3	10.3	Illite	Illite	Amphibole
1936	10.3	10.3	10.3	Illite	Illite	Amphibole
1948	10.3	10.3	10.3	Illite	Illite	Amphibole
2006	10.3	10.3	10.3	Illite	Illite	Amphibole

APPENDIX II: Results of the XRD analysis for Well MW-12

Depth (m)	D(001) Untreated	D(001) Glycolated	D(001) Heated	Mineral	Type	Other minerals
590				No clay		Amphibole
810				No clay		
1498				No clay		Possible kaolinite,amphibole
1630	10.4	10.4	~10,4	Illite	Illite	Amphibole
1666				No clay		
1700	10.3	10.3	10.3	Illite	Illite	Amphibole
1736	13.4/10.3	13.4/10.3	~10	Sm: sm/ill	Smectite-Illite	Amphibole
1860	12.8/10.3	12.8/10.3	~10	Sm: sm/ill	Smectite-Illite	
1872	17.7/10.3	17.7/10.3	~10	Sm: sm/ill	Smectite-Illite	

APPENDIX III: XRD patterns for the clay minerals in wells MW-09 and MW-12

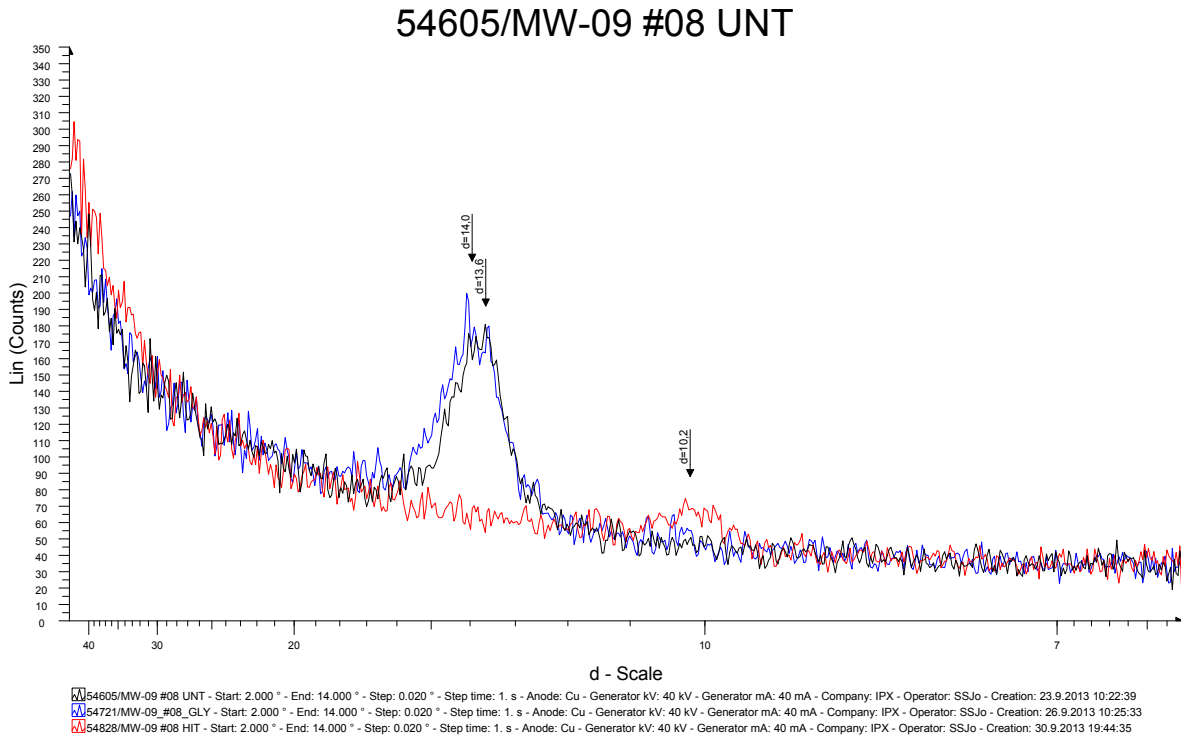

FIGURE 1: Smectite at 820 m

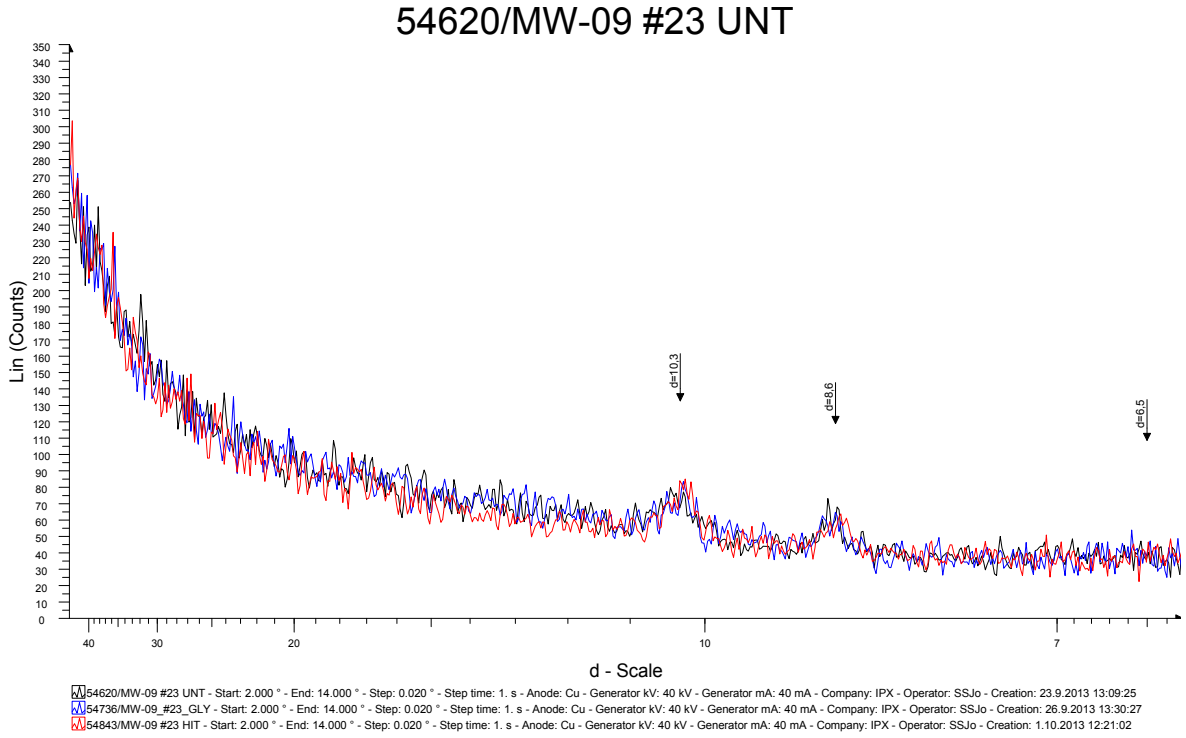

FIGURE 2: Illite, amphiboles and feldspars at 1844 m

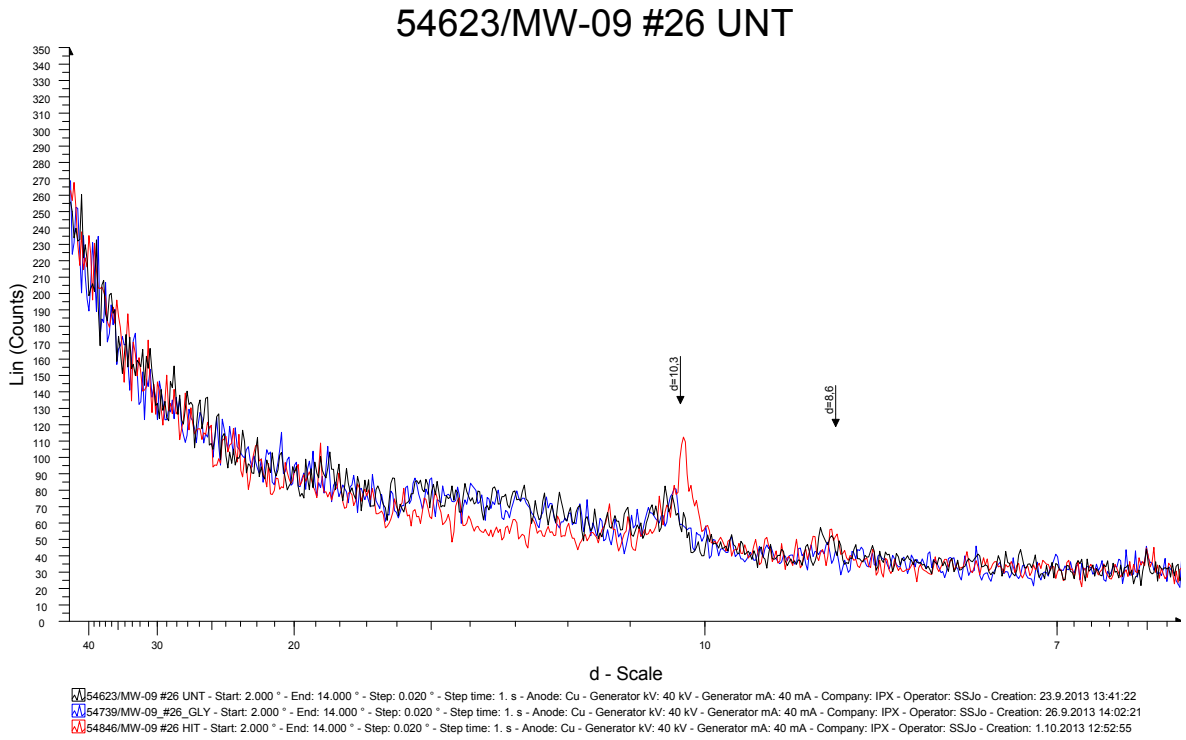

FIGURE 3: Illite and amphiboles at 1946 m

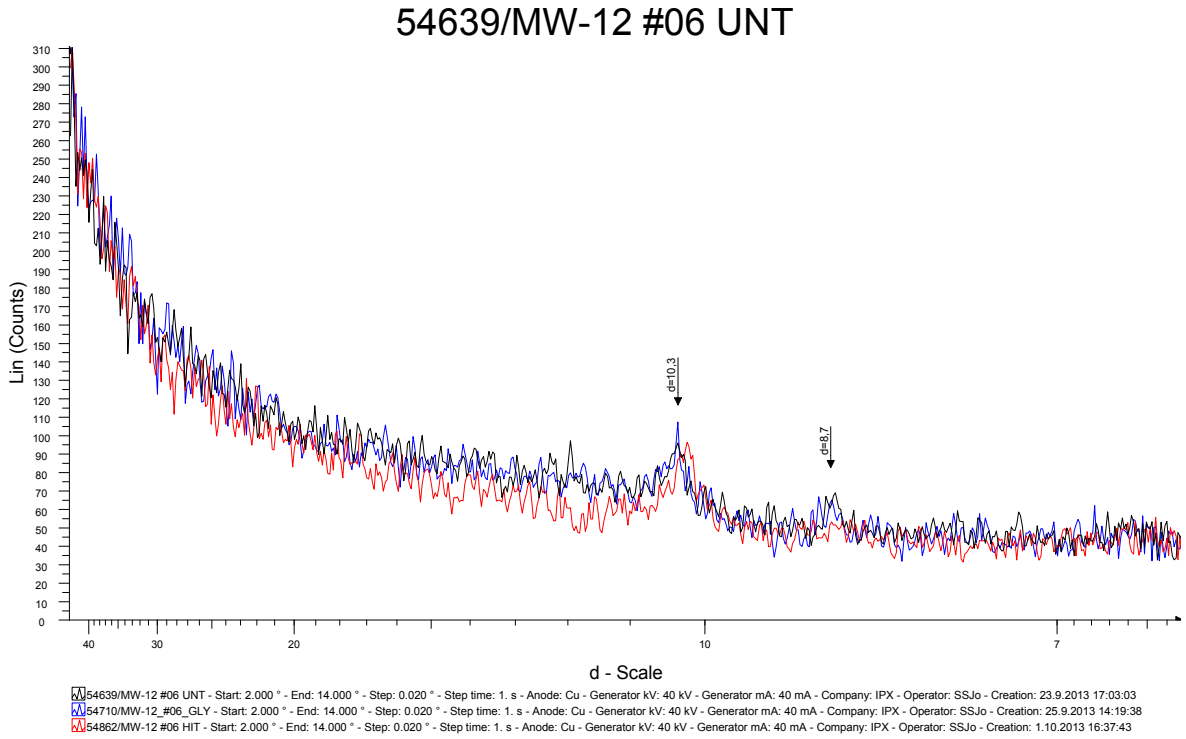

FIGURE 4: Illite and amphiboles at 1700 m

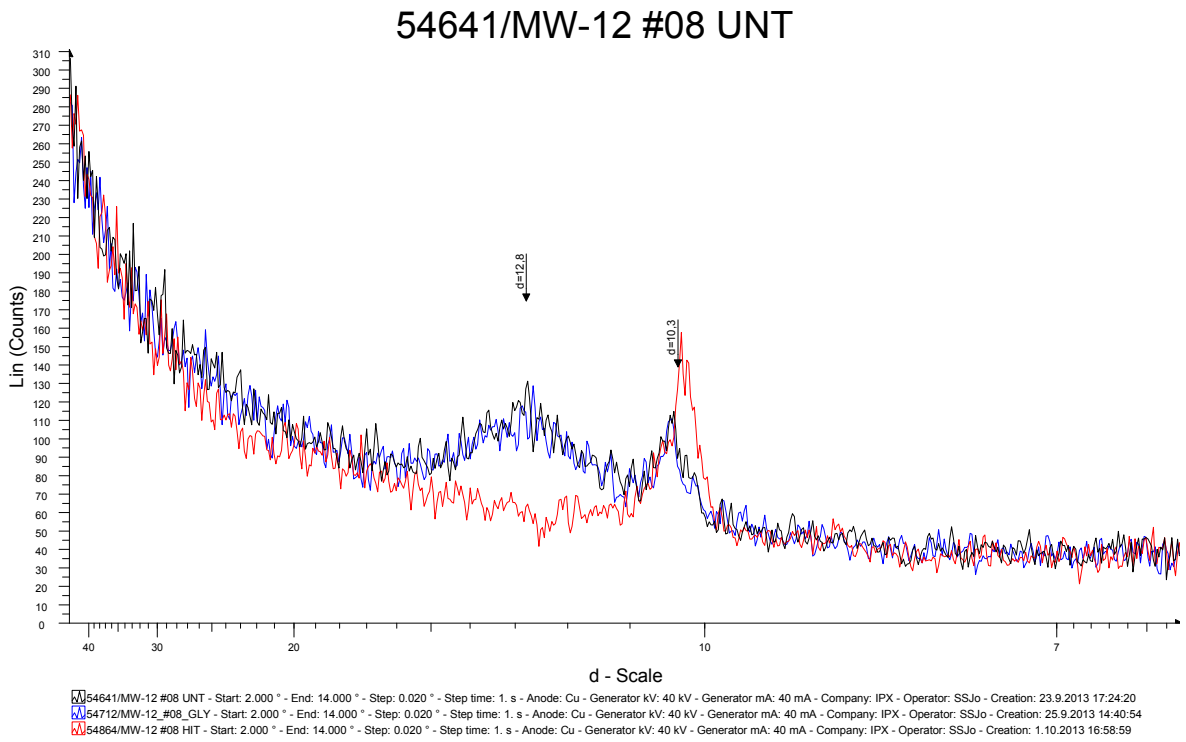

FIGURE 5: Illite and smectite at 1736 m